Tidal asymmetry and flood/ebb dominance in deltas: the Sibsa-Pussur estuary, Bangladesh

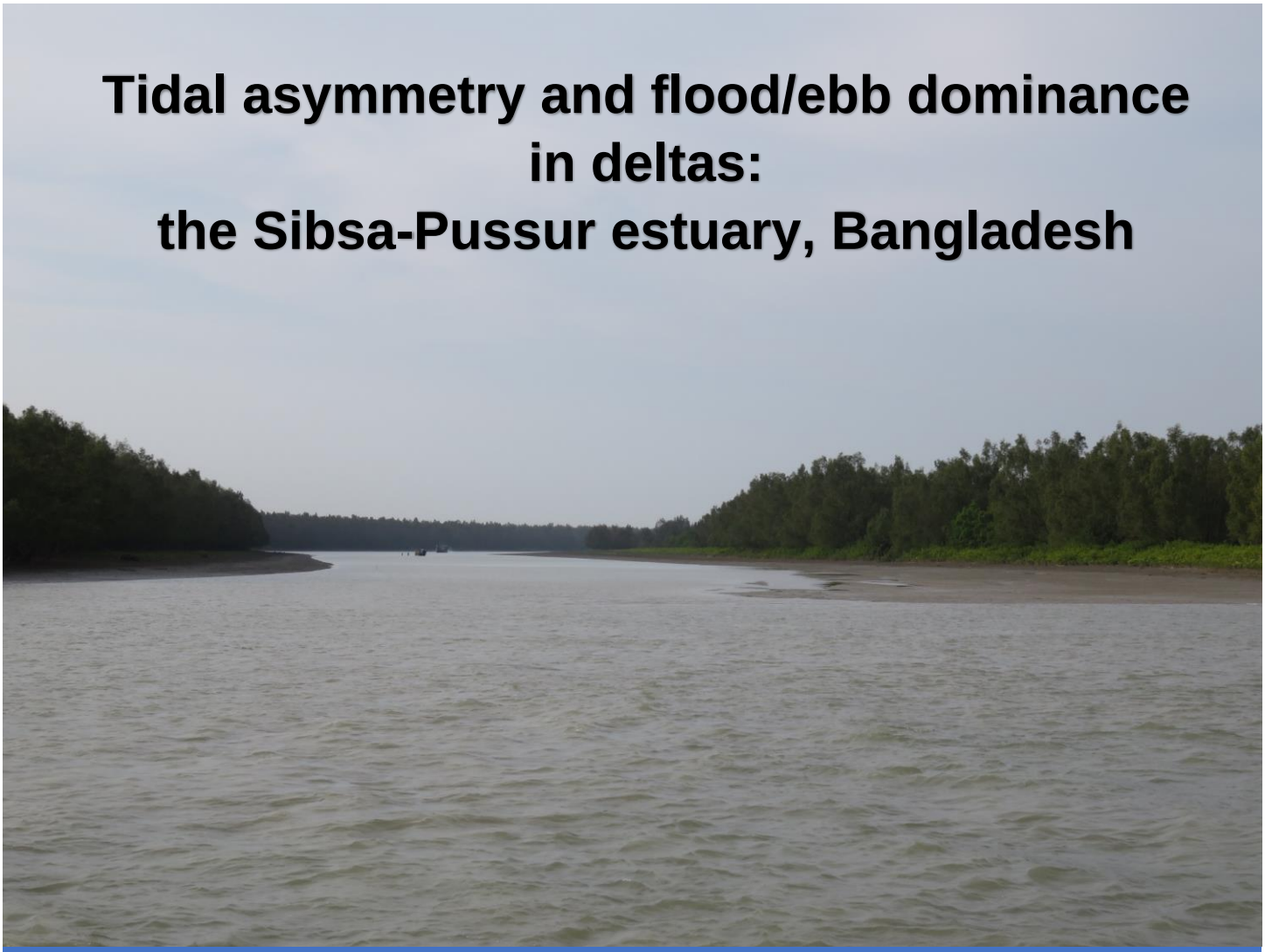

MSc thesis

Md Nurul Kadir (920202416120)

Supervised by Reinier Schrijvershof and A.J.F. (Ton) Hoitink

Hydrology and Quantitative Water Management Group,

Wageningen University and Research

15 March 2021

WAGENINGEN
UNIVERSITY & RESEARCH

Abstract

Tidal asymmetry in deltas, resulting from the combination of astronomical tides and nonlinear tidal interactions in shallow water, plays vital roles in sediment transport in the estuaries. Quantification of tidal asymmetry is essential for understanding the factors contributing to long-term morphological changes. In this study, the harmonic analysis method (T_tide) is applied to examine the spatiotemporal evolution of tidal asymmetry under strongly variable river discharge conditions in the Sibsa-Pussur (SP) estuary of the GBM delta. The required data is generated using a hydrodynamic model (Delft-3D) for the year 1978, 1988, 2000 and 2011. The eight main tidal constituents (M2, M4, M6, K1, S2, O1, MS4, MSf) are considered for data analysis. The tidal duration asymmetry and peak current asymmetry are determined, and the results quantify the tidal asymmetry based on the amplitude ratio and phase difference. The results show that the SP estuary becomes flood dominant over time, where the Pussur river shows more maximum flood dominant tidal asymmetry than the Sibsa river. The upstream river discharge has enormous influences on the tidal regime of the SP estuary. Decreasing discharge towards the SP system increased the flood dominant conditions. Including morphological changes in the model may improve the model results, which will help to understand the main reason behind the SP estuary's sedimentation problem more accurately.

Table of Contents

1 Introduction

1.1 Context and Motivation

Deltas are very popular places to live because of their prosperous fertile lands, productive fisheries, and other ecological and economic values (Guo et al., 2016). This populous nature of deltas necessitates various infrastructure projects for flood protection and land reclamation for agriculture and other uses. Typical measures include polderization and the building of dams/barrages for diverting river water for irrigational purposes. Reclamation works often result in serious environmental problems, including loss of biodiversity, deterioration of coastal water quality, and depletion of fishery resources (Son & Wang, 2009). The direct impacts of these human interventions are preventing the natural process of land elevation rising and inducing subsidence (Li et al., 2010). Furthermore, embankments alter the planform shape and cross-sectional geometry of the tidal rivers, creating strongly convergent estuaries and reducing the extent of intertidal area (Stark et al., 2017).

Like other deltas, the coastal zone of the Ganges-Brahmaputra-Meghna (GBM) delta was also subjected to extensive human interventions in the past decades to accommodate the growing population (Auerbach et al., 2015). These human interventions are; the construction of polders, (partial) closure of distributary rivers, changes in upstream sediment loads and reduction of discharge during the dry period, resulting from reservoir construction (Wilson et al., 2017). This results in an intricate pattern of local erosion (Auerbach et al., 2015), infilling of tidal channels (Wilson et al., 2017) and amplifying tidal amplitudes (Pethick & Orford, 2013). The hydrodynamic and sediment transport processes dictating the morphological development in these systems varies enormously. The eastern part of this system is freshwater dominated as it is the endpoint of the GBM basin (Figure 1.1). These three mighty rivers carried more than a billion tons of total sediment/year and discharged into the Bay of Bengal (Rahman et al., 2014). A significant portion of this sediment redistributed again within the nearest estuaries (Rahman et al., 2018). On the other side, the western part (consisting of two major rivers Sibsa and Pussur) of this delta is tide-dominated (Bomer et al., 2019), which allows carrying the sediments from the sea to the rivers.

This region is also affected by the upstream barrage construction; named Farakka barrage (operating from 1975) (Rahman & Rahaman, 2018). The Farakka barrage diverts water from the Ganges river to the Hooghly River of Kolkata (District of India). Consequently, it reduces the flow in the Gorai river (Figure 1.1), which is the primary freshwater source for the western region. Rahman and Rahaman (2018) show that the monthly averaged discharge of the Gorai river has been reduced by around 50% in the dry season (January – May) due to this barrage. The anthropogenic interventions have altered the natural dynamics and created various problems like; channel siltation, lowering the adjacent tidal-plain and floodplain (subsidence), and channel abandonments in the south-west region of the country. About 600 km of this region's major waterways were infilled in recent decades due to sedimentation and/or direct waterways blocking (Wilson et al., 2017). Ultimately, it reduces the navigability of that region (Angamuthu et al., 2018).

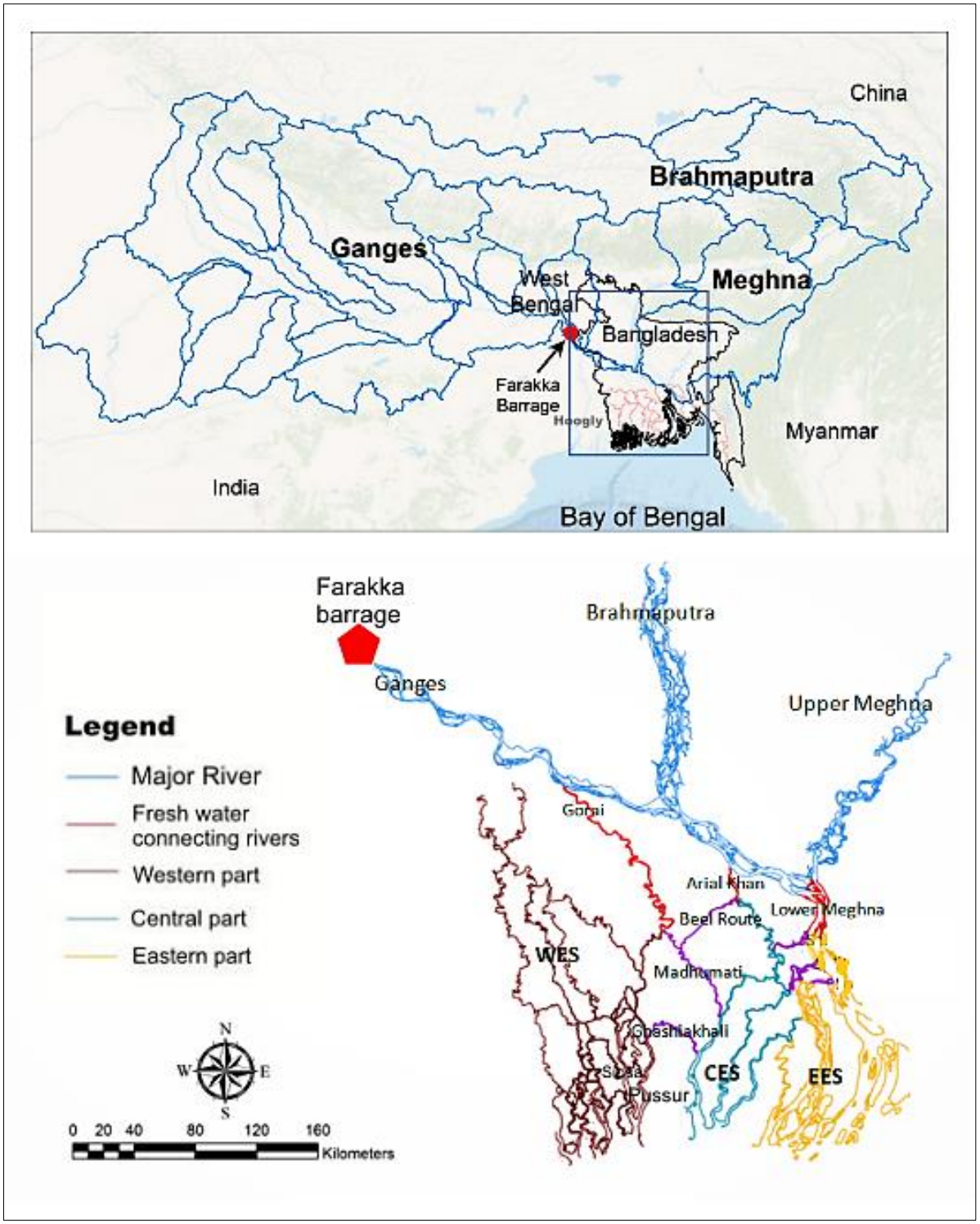

Figure 1.1 The Ganges-Brahmaputra-Meghna Delta, including the connectivity among the rivers with the location point of the Farakka barrage.

Due to this sedimentation, many small connecting channels (upstream of the Sibsa river) are filled up and lost their connection with the Ganges system (Mirza, 2004). As a result, a single existing channel remains for connecting the Gorai river with the Pussur river (Figure 1.1). That is why, though the Pussur receives some freshwater discharges, but the Sibsa does not. Despite that, the Pussur system has recently become accreting contrary to the Sibsa system. Which also leads to a continuous dredging activity in the Pussur system. The exact mechanisms driving the increased channel siltation is not fully understood yet. The contrary behaviours of these two tidal rivers (Sibsa and Pussur) are needed more insights for maintaining the navigability of these rivers in the future. On top of these local interventions, the GBM delta is also subject to sea-level rise (SLR), consisting of a global component (including the anticipated acceleration in SLR), which can exacerbate this problem even more.

From previous studies in different deltas, it is found that the deformation of the tidal wave is closely linked to geometrical channel properties (Quesada et al., 2019; Rossi & Steel, 2016; van Rijn, 2011). When tidal waves propagate into shallow estuaries, they are modified by landward width convergence and depth reduction, bottom friction, and river discharge (Lanzoni & Seminara, 1998). The width convergence factor mainly determines the amplification of the tidal wave while the presence of intertidal areas (acting as intertidal storage volume and a source of friction) reduces the high-water wave propagation celerity and influences tidal amplification (Toffolon & Lanzoni, 2010). Ultimately, these kinds of tidal interactions with basin geometry, bathymetry, and river flow lead to asymmetric tides (Parker, 2016). Tidal asymmetry associated with the tidal distortion can significantly affect net sediment transport, and consequently, estuary evolution and stability (Dronkers, 1986; Friedrichs & Aubrey, 1988; Jiang et al., 2011; Speer & Aubrey, 1985). Therefore, analysing the tidal asymmetry in the Sibsa-Pussur system can help to understand the reason behind the siltation problems. It will also give the opportunity to see the effect of different anthropogenic activities on this estuary.

1.2 Research Objectives

This MSc thesis focusses on the historical changes of tidal dynamics in estuaries, which is further complicated by changing upstream boundary conditions. The Sibsa and Pussur river system of Bangladesh is used as a case study. With the help of a numerical model (Delft3D), different years of hydrodynamic changes are studied. This study aims to assess the changes of tidal asymmetry in the Sibsa-Pussur estuary, considering this is the primary driving mechanism for sediment import/export, and establish the influence of river discharge variation on tidal asymmetry.

1.3 Research questions

Through this research, the following questions will be answered.

1. How has tidal asymmetry developed in the Sibsa-Pussur estuary?
2. What are the differences in tidal asymmetry between the Sibsa and Pussur river?
3. How does river discharge modulate the tidal regime?

2 Theoretical Background

2.1 Tidal wave propagation in shallow water:

Astronomical tides are originated from the combined gravitational forces of the moon and the sun. The frequencies of tidal constituents in the oceans directly relate to lunar or solar days, which can be denoted in terms of diurnal and semi-diurnal components. The propagation of tides in the deep ocean is primarily governed by linear processes, where their interactions generate subharmonic tides (spring-neap cycle) (Gallo & Vinzon, 2005). The main semi-diurnal tidal constituents are M2 (Principle lunar) and S2 (Principle solar), and the main diurnal tidal constituents are K1 (Luni-solar diurnal) and O1 (Principle lunar diurnal). In shallow coastal waters (where the depth is less than 200m), other nonlinear forces and processes such as bottom friction, diffusion (due to turbulence), and advection (due to advective inertia forces) become increasingly accountable for the dynamics of the tides. These non-linear process, such as bottom friction, which depends on the square or higher power of the tidal signal, modify the tidal wave on the shelf. As a result, the tidal signal is become more complicated and can no longer be represented by simple linear superposition of semi-diurnal and diurnal components. Using the Fourier series concept, this nonlinear tidal signal can be reconstructed by combining higher-frequency tidal components or superharmonic tides. The nonlinear interaction of an astronomical tidal component with itself generates overtides with higher frequencies such as M4 (2ωM2), M6 (3ωM2), S6(3ωS2). Furthermore, the interaction with other tidal components generates compound tides, viz. MS4 (ωM2+ωS2), MN4(ωM2+ ωN2) etc. (Neill & Hashemi, 2018)

2.2 Characterising tidal asymmetry

Overtides and compound tides are the main causes of tidal asymmetry (Piano et al., 2017). Several methods are present to characterise and quantify tidal asymmetry (such as the harmonic method, statistical method) (Guo et al., 2019). In this study, the harmonic method is considered only. The harmonic method is based on the phase differences and amplitude ratios of the interacting tidal constituents. The strength of the asymmetry depends on the ratio between the amplitude of the semi-diurnal tide and the overtides (M4/M2, M6/M2). Furthermore, the nature of asymmetry (whether ebb- or flood-dominance) is determined by the phase difference between tidal constituents (Ø= 2M2-M4) (Figure 2.1 & 2.2).

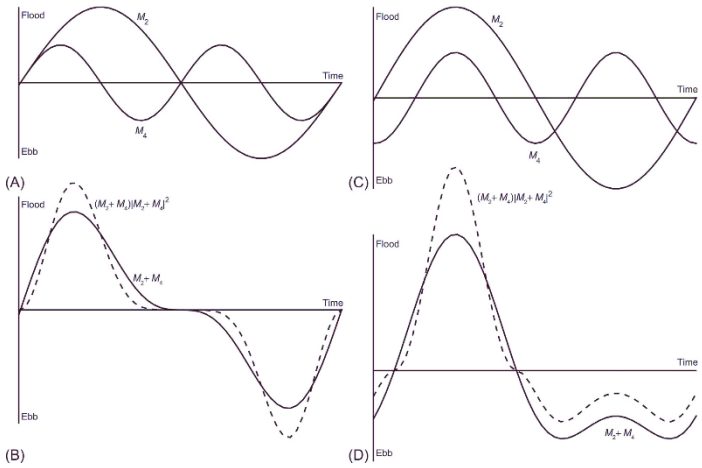

Figure 2.1: Contributions of M2 and M4 tidal constituents leading to (B) a distorted but symmetrical tide and (D) tidal asymmetry. In (A), the phase lag between M2 and M4 is 0 degrees, and in (C) the phase lag is 90 degrees. (adapted from: Neill & Hashemi, 2018)

In general, the phase relationship between the principal semi-diurnal tide (M2) and it's first harmonic (M4) dominates the tidal asymmetry (Friedrichs & Aubrey, 1988). Although the combination of M2 and M4 tidal currents in Figure 2.1A results in a distorted tide (Figure 2.1B), whether it is symmetric or asymmetric depends on its phase difference (Figure 2.1C & 2.1D). Tidal asymmetry can be interpreted as the vertical and the horizontal tides: the vertical tide refers to the water elevation, and the horizontal tide refers to the tidal flow velocity. In the estuarine system, shallow water influences them both. Within an estuary, the principle of distorted tidal height "A" and tidal velocity "V" can be illustrated as;

$$A = a_{M2}cos(\omega t - \theta_{M2}) + a_{M4}cos(2\omega t - \theta_{M4})$$

$$V = v_{M2}cos(\omega t - \varphi_{M2}) + v_{M4}cos(2\omega t - \varphi_{M4})$$

where t is time, ω is tidal frequency, a is the amplitude of tidal height, v is the amplitude of tidal velocity, θ is the phase of tidal height, and φ is the phase of tidal velocity. The vertical tide phase difference between M2 and M4 is defined as;

$$\emptyset = 2M2 - M4 = 2\theta_{M2} - \theta_{M4}$$

And the tidal amplitude ratio can be defined as

$$M4/M2 = a_{M4}/a_{M2}$$

Similarly, the non-linear parameters for tidal velocity are $2\varphi_{M2} - \varphi_{M4,}$ and v_{M2}/v_{M2}. An undistorted tide has M4/M2 amplitude ratios of zero. A distorted but symmetric tide has a relative 2M2 – M4 velocity phase of ±90° and M4/M2>0 for horizontal tides (Figure 2.2). If the velocity phase ranges from -90° to 90°, then the distorted composite tide has a higher velocity flood and is defined as flood-dominant.

A system is called a flood dominant when the falling tide's duration exceeds the rising tide (Kennish, 2016). If the falling tide duration is shorter than the rising tide, it leads to a stronger peak ebb current and the system is referred to as ebb dominant (Kennish, 2016), and the velocity phase ranges from 90º–270º (Figure 2.2). For vertical tide, the flood dominant phase difference ranges from 180º-360º, and the ebb dominant phase difference ranges from 0º - 180º (Figure 2.2).

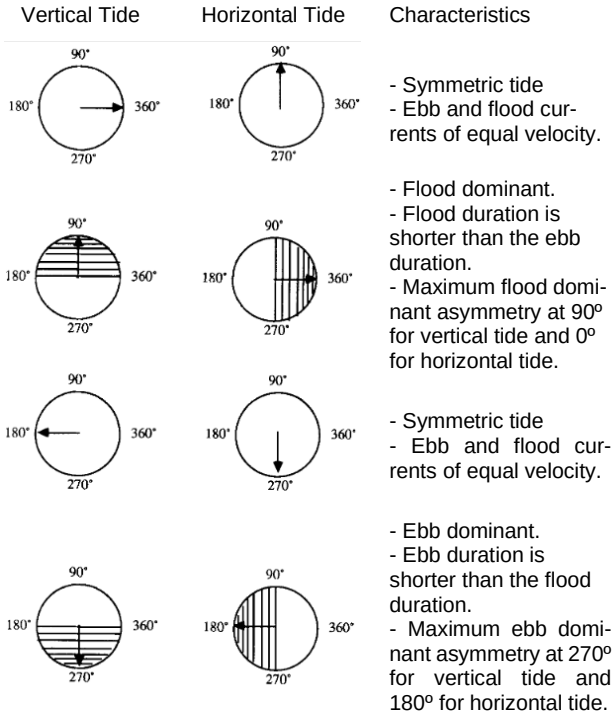

Figure 2.2: Linear relationships between relative phase and tidal distortion for M4/M2>0 (Adapted from Friedrichs & Aubrey, 1988)

2.3 Tidal asymmetry and sediment transport

Tidal asymmetry is considered one of the most critical processes in creating residual sediment transport and associated large-scale morphological changes in tidal environments, including estuaries (Gong et al., 2016). Based on its mechanism, tidal asymmetry can be different, such as (1) unequal rising and falling tidal duration of vertical tides, caused tidal duration asymmetry (TDA); (2) uneven peak ebb and flood velocities, caused peak current asymmetry (PCA); and (3) unequal high water and low water slack durations in tidal currents, caused slack water asymmetry (SWA) (Dronkers, 1986; Gong et al., 2016; Guo et al., 2019). Based on the nature of tidal

asymmetry, it can be flood dominance or ebb dominance. A shorter rising tide than the falling tide, stronger peak flood currents than ebb currents, or longer high water slack than low water slack result in flood dominance. On the contrary, a shorter falling tide, stronger ebb currents, or longer low water slack promote ebb dominance (De Swart & Zimmerman, 2009). A flood tidal asymmetry induces a landward residual sediment transport (sediment import from the sea), and an ebb tidal asymmetry causes a seaward residual sediment transport (sediment export to the sea) (Guo et al., 2014).

Sediment transport rates “s”, generally scale with the power function of tidal currents “u”; ($s=fu^x$, where x varies from 3 to 5), so slight differences between flood and ebb currents can cause significant residual transport differences (De Swart & Zimmerman, 2009; Dronkers, 1986; Postma, 1961). The transport behaviour of bedload (e.g., sand) and suspended load (e.g., silt and clay) are different. The bedload sediment transport rate is mainly the power function of current velocities with little time lag effects. Simultaneously, the suspended load is mixed throughout the water column and strongly affected by time lag effects on initial motion and settling (Groen, 1967; Postma, 1961; Van Rijn, 1993). Different indicators of residual sediment transport are developed based on tidal asymmetry. The peak current asymmetry (PCA) serves as an indicator of a residual flux of coarse sediment, and the slack water asymmetry (SWA) serve to indicate the residual flux of fine sediment (Dronkers, 1986)

In practice, PCA and SWA are not easily computed because long records of tidal currents are not readily available. Thus an alternative indicator is tidal duration asymmetry (TDA), characterising inequality between rising and falling tidal periods in tidal water levels. TDA is much more widely used because of the availability of tidal water level data. However, TDA is not an alternative for PCA. Tidal currents are far more sensitive to basin geometry (e.g., channels, shoals and tide flats) and external forcing (e.g., river discharge) than surface water heights; thus, PCA is still preferred in indicating residual sediment transport. In this study, both the tidal duration asymmetry (as asymmetry of the vertical tide) and the peak current asymmetry (as asymmetry of the horizontal tide) are determined.

3 Methodology

This section describes the methodology to answer the research questions, starting with the selection of the study area and a detailed description of the field site (section 3.1). Then the collection of the available data are described in section 3.2. Availability and quality of the field data lead to a hydrodynamic model, which is discussed under the model description (section 3.3). Last section 3.4 will describe the use of the T-tide function (developed by Pawlowicz et al., 2002) to determine the tidal amplitudes and phases. Figure 3.1 shows the methodological framework of this study.

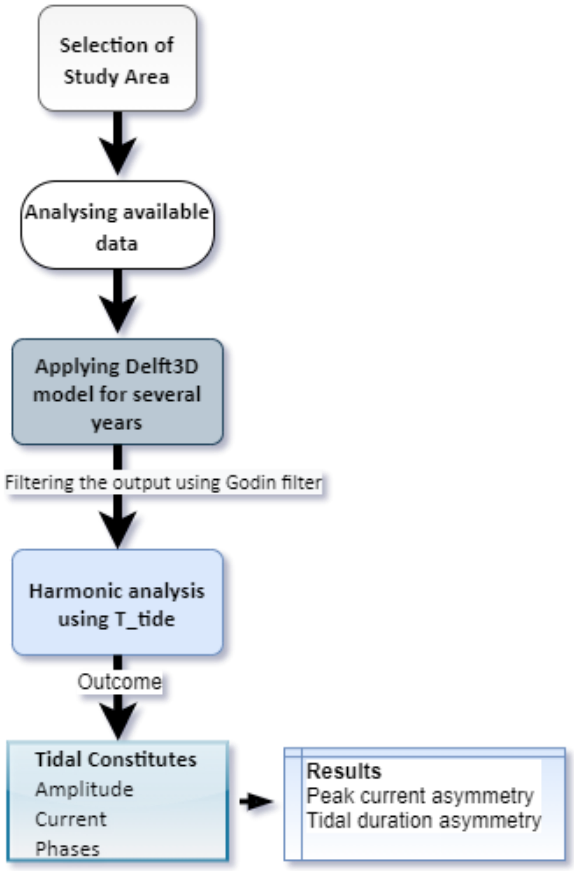

Figure 3.1: Methodological framework of the study.

3.1 Site Description

The western part of the lower GBM delta is considered for this study. This part is characterised as an extensive system of tide-dominated rivers (distributaries of Ganges). The main two rivers in this part are Sibsa and Pussur rivers. These are connected to the Ganges by the Gorai and partly by the Madhumoti and the Arial Kha rivers (Figure 1.1). So, the flow in these systems directly depends on the Ganges river flow.

In 1971, the Farakka Barrage was built across the Ganges at the Ganges delta's apex (Start operating from 1975) (Figure 1.1). This barrage aims to divert 1,800 cubic metres per second of water from the Ganges to the Hooghly River for flushing out the sediment deposition from the Kolkata harbour. Because of that, flow in the Gorai distributary of the Ganges reduced significantly over the last few decades (Rahman & Rahaman, 2018). Which ultimately decrease the water flow towards the Sibsa-Pussur (SP) system.

The second-largest seaport of Bangladesh, known as Mongla seaport (approximately 132 km upstream from the sea), is located on the east bank of the Pussur river (Figure 3.2). Since its establishment in 1950, this port has been playing an important role in international trade, national defence, and commerce of the country (Islam & Haider, 2016). It is necessary to maintain the navigability (at least 7.5 m navigable draft) of these rivers to keep this port active throughout the year. Because of that, several dredging efforts have been made to restore the navigability of the Pussur River (Rahman & Ali, 2018).

The construction of polders is also present in this system. During 1960, East Pakistan Water and Power Development Authority (called EPWAPDA that time, now known as BWDB) constructed over 139 polders (4000 km of embankments) across the entire coastal belt of Bangladesh (BWDB, 2013). These polders were built to protect the land from coastal flooding, storm

surges and help achieve food security through better water control. In the south-western part alone, about 1566 km of embankments (polders) were constructed (BWDB, 2013). Therefore, many anthropogenic interventions have affected the natural system of this area over the past five decades.

This system is also crucial for the presence of the mangrove forest “Sundarbans” (Figure 3.2). A significant part of the system runs through this forest. These extensive vegetated areas also have an enormous influence on tidal propagation.

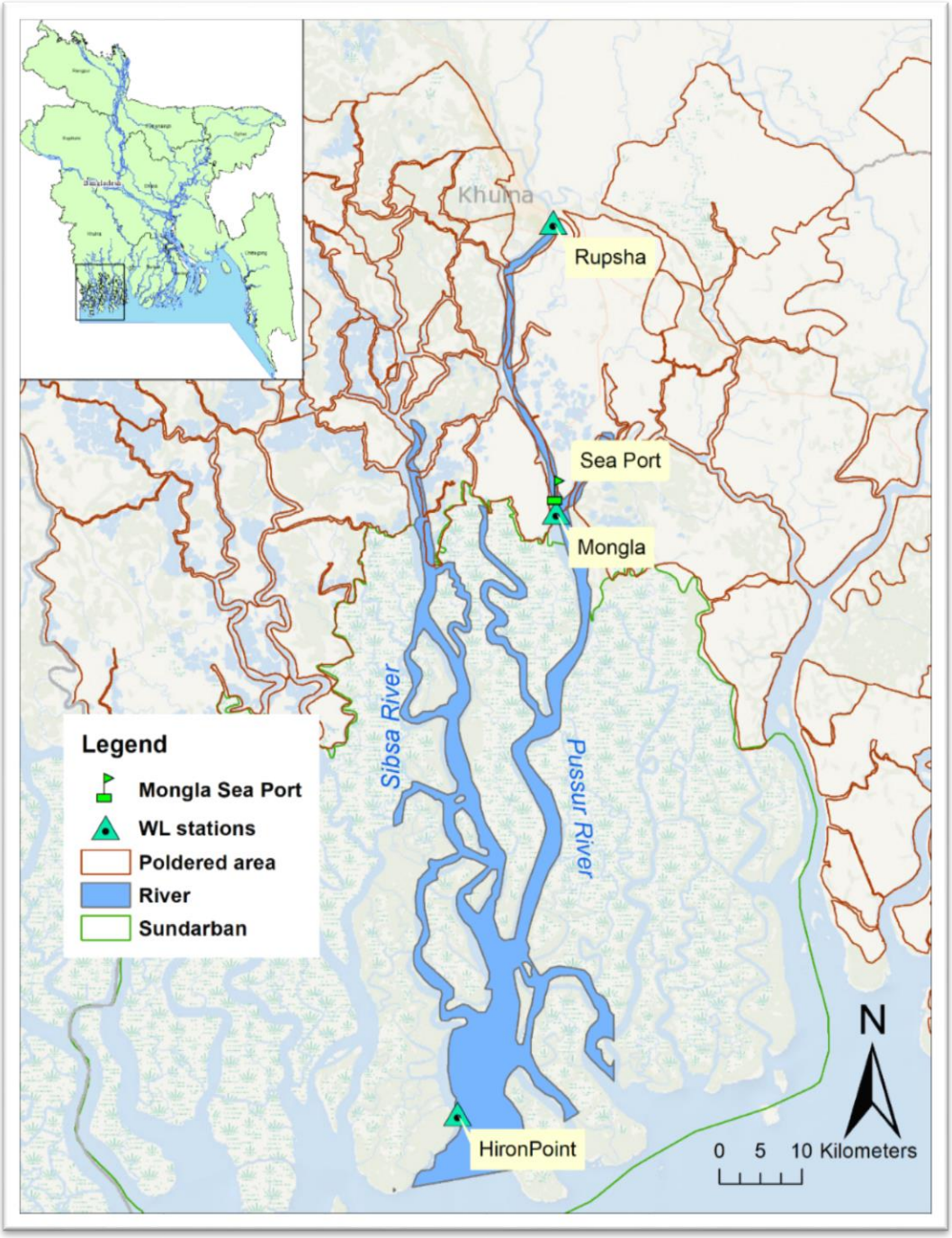

Figure 3.2: Location map of the Sibsa-Pussur river with existing Water level stations, Polders, Mongla seaport, and the Sundarbans.

3.2 Data Collection

All the data used in this study are collected from secondary sources. Two governmental organisations, the Bangladesh Inland Water Transport Authority (BIWTA) and the Bangladesh Water Development Board (BWDB), are responsible for collecting water level (WL) data of the river in the study area. BIWTA measures the Data using the automated gauge at 30minutes intervals, and BWDB manually took the high tide and low tide WL of a day (two readings in a day).

BIWTA has two WL measuring stations (Figure 3.2) within this study area. (i) The Hironpoint station, located closest to the ocean with data available from the year 1977 to 2015, and (ii) The Mongla station, located near the Mongla seaport (Figure 3.2), which data are available from the year 2000 to 2015 with some missing values in between. The Rupsha station, operated by the BWDB, is situated in the most inland (Figure 3.2). This station's data are available from the year 1981 to 2012.

The tidal regime of the Sibsa-Pussur system is calculated by using the Hironpoint observed data. Hoitink et al., (2003) classified the world's tidal regimes based on the tidal form number F, [$F=(A_{K1}+A_{O1})/(A_{M2}+A_{S2})$, where A is the tidal amplitude of corresponding tidal constituents] Tides are defined as diurnal for F > 3 and semi-diurnal for F< 0.25. The mixed tides in-between are dominantly semi-diurnal for F= 0.25-1.5 and dominantly diurnal for F= 1.5-3. In this study, the SP estuary's tidal form number found as 0.23, which is in the semi-diurnal regime (F ≤ 0.25).

In general, the tidal asymmetry tends to flood dominant in most semi-diurnal regimes (Song et al., 2011). However, further tidal analysis is necessary to know about the strength and the nature of the tidal asymmetry. With the available data range and data period, it is hardly possible to perform the tidal analysis. Therefore, a hydrodynamic model is used to generate more frequent water level and velocity data. The velocity data is necessary to calculate the tidal asymmetry of the horizontal tide.

3.3 Model Description

A hydrodynamic Delft3D model of the Pussur-Sibsa system is developed by Deltares (van Maren, 2020) and made available for this study (Figure 3.3). Delft-3D is a grid-based structured model capable of simulating the hydro-morphodynamical changes of a system (Deltares, 2014).

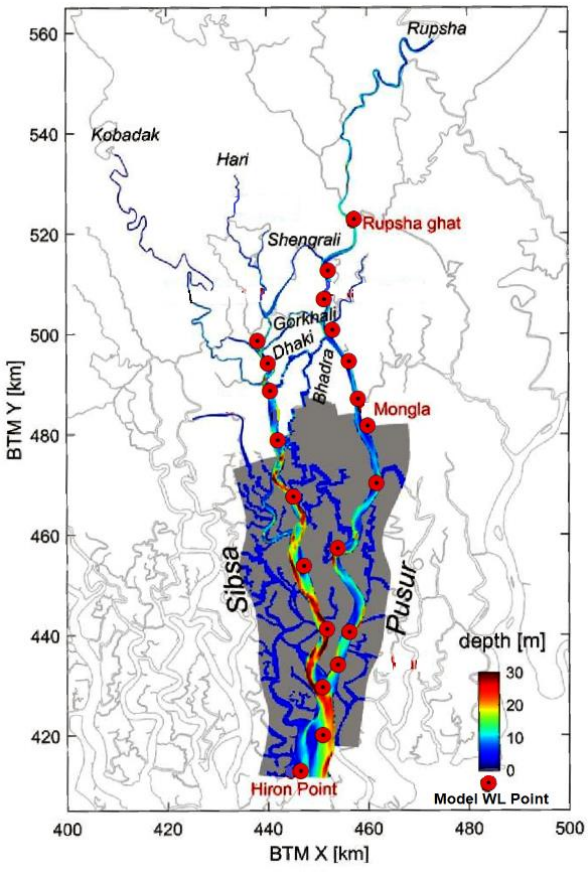

Figure 3.3: Model domain (in colours) with names of the existing observation stations (in red) and main rivers (black italics). The grey areas are the vegetated Sundarbans, with a depth of 2 meters above MSL. Depth is relative to MSL. (Adapted from van Maren, 2020)

For this study, only hydrodynamic changes are considered to generate both spatial and temporal data. Twenty-one observation points over the study area (Figure 3.3) are considered to generate the hydrodynamic (water level and velocity) data for the year 1978, 1988, 2000 and 2011.

The model boundaries were forced with water levels at Hironpoint and discharge from the upstream rivers “Nobaganga”, “Hari”, and “Kobadak” (Figure 3.3). The upstream river's discharges were collected from the Institute of Water Modelling (IWM) Bangladesh (Figure 3.4). From the available discharge data, it is found that Nobaganga supplies a significant portion of the water to the SP system and receive this water from the Gorai river (Figure 1.1). The contribution from the Hari and Kobadak rivers are minimal in amount.

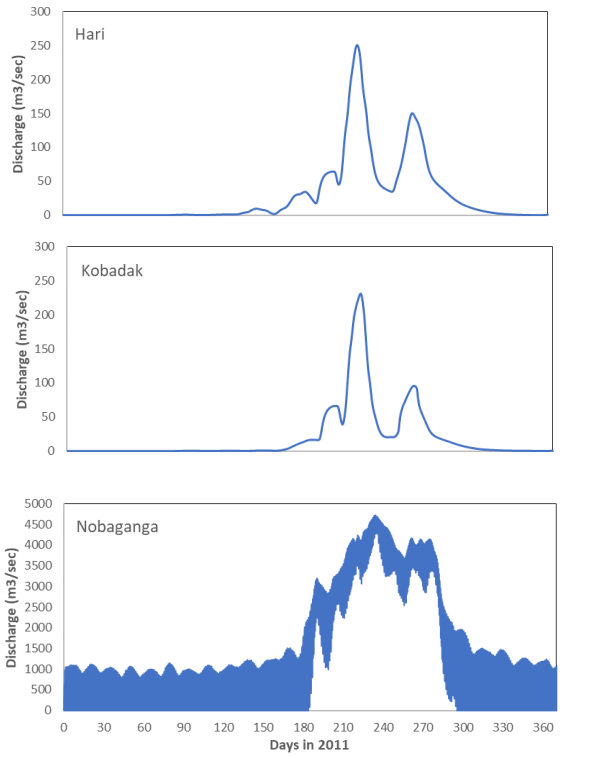

Figure 3.4: Boundary conditions for the Nobabanga, Kobadak and Hari Rivers.

The SP model was calibrated against water levels (Figure 3.5a) and discharge (Figure 3.5b). In both cases, Manning’s n was considered as a calibrating factor. The run with the manning’s n = 0.015 shown the most satisfactory results in both cases (Figure 3.5), which is considered for further model use.

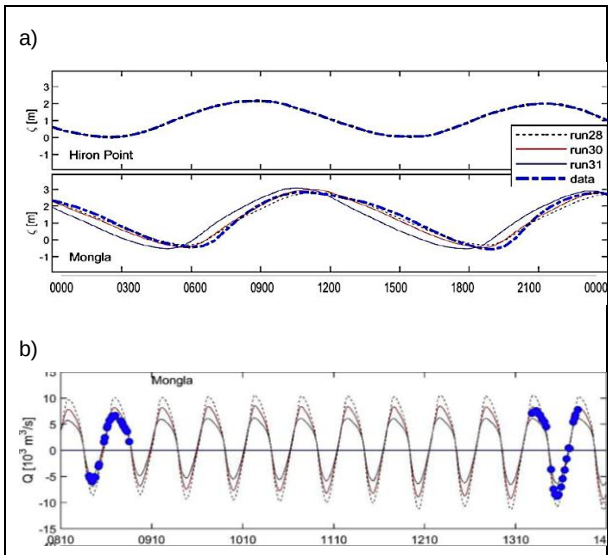

Figure 3.5: Computed and Observed (a) water levels and (b) discharges, Run 28 represents the Manning’s n = 0.015. (Source: van Maren, 2020)

The calibrated SP model is used for further data generation. The model was run for years 1978, 1988, 2000, and 2011 to represent the 40 years of temporal variation. For each year run, only the boundary conditions (both upstream and downstream) of the model were changed as there corresponding years. All the other model settings and bathymetry were kept the same as the calibrated model. Furthermore, 21 observation points (12 at Pussur, 08 at Sibsa channel, and 01 at Hironpont used in common) were considered for the spatial tidal analysis (Figure 3.3).

Two hypothetical upstream boundary condition was created to observe the effect of upstream discharge variation on the system. One referred to as “1.5Q”, which means hypothetically discharge increased by 1.5 times of the actual

discharge in the dry time. This increment factor is chosen because Rahman & Rahman (2018) found that during the dry period, the Farakkha barrage reduced the river's average discharge by about 50%. So, considering no Farakkha barrage will increase the flow by 1.5 times. Another one referred to as “2Q”, which means two times the discharge increased during the dry time. This scenario was developed to see how the system will act if more water is allowed from the upstream.

3.4 Tidal Analysis

The tidal analysis is necessary for determining the tidal asymmetry of a system. Harmonic analysis is the most common tidal analysis method, which provides quantitative metrics to analyse the tides. For that, a least-squares tidal analysis (T_tide; Pawlowicz et al., 2002) is used to separate the main tidal constituents' amplitudes and phases. With that, to see the impact of river discharge, the nonstationary harmonic analysis is done using NS_tide (a modified version of T_tide, developed by Matte et al., 2014). Before using the model output in tidal analysis, it is required to remove the high-frequency signal from the time-series data to get a more accurate tidal analysis result. For that, the Godin filter was used to remove the high-frequency signal (Godin, 1972).

3.4.1 Data filtering

The “Godin_Filter” function was used for both the WL time-series data (Figure 3.6a) and the velocity (both “u” and “v” components) time-series data (Figure 3.6b). According to Godin (1972), this function applies a three-step low-pass filter to a time-series to remove the higher frequency signals and obtain the residual signal.

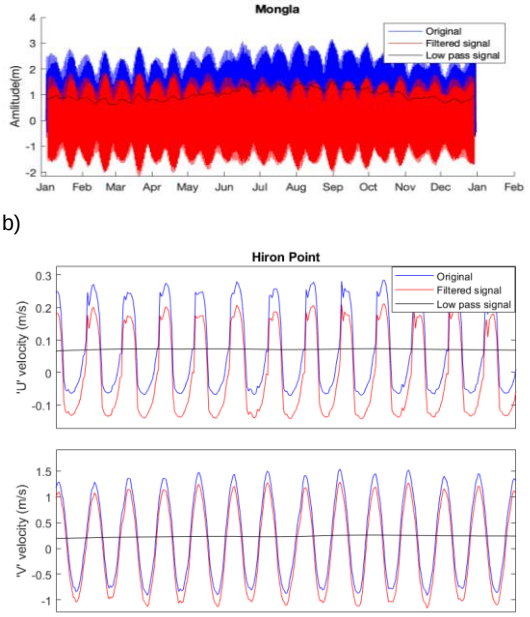

Figure 3.6: Godin-filtered time series (red line), original/model output time series (blue line), and residual series (black line) for a) water level at Mongla, b) Expanded velocity time series at HironPoint station.

After getting the filtered time series value, the T_tide function was used for doing the Harmonic analysis.

3.4.2 Applying T_tide:

T_tide uses an equilibrium tide model to obtain frequencies of tidal constituents, then fits each of these constituents to the provided time series and finds each constituent's best-fit phase.

T_tide models the tidal heights ζ as

$$\zeta(t) = f_{0,0} + \sum_{i=1}^{n} [f_{1,i}\cos(\omega_i t) + f_{2,i}\sin(\omega_i t)]$$

Where t is time, ω_i is the frequency of an individual tidal constituent, and $f_{0,0}$, $f_{1,i}$ and $f_{2,i}$ are unknown coefficients to be determined by regression analysis using observations (Pawlowicz et al., 2002).

The T_tide function allows for analysing scalar data (heights, figure 3.7a) and complex data (velocity, figure 3.7b). The Delft3D model can generate the depth-averaged velocity at a given observation point. This velocity is formed as complex data with the “U” and “V” component. All the model's observation points are located on the thalweg of the river. That is why the depth-averaged velocity of the corresponding observation point is considered representative of the whole cross-section. During the harmonic analysis, the T_tide function calculates the magnitude of the complex data as; U+sqrt(-1)*V (where U is the eastward velocity and V is the northward velocity)(Pawlowicz et al., 2002).

Figure 3.7 shows the output obtained from T_tide for the analysis period of 2011. The model prediction of T_tide fits well with the filtered data (Figure 3.7a).

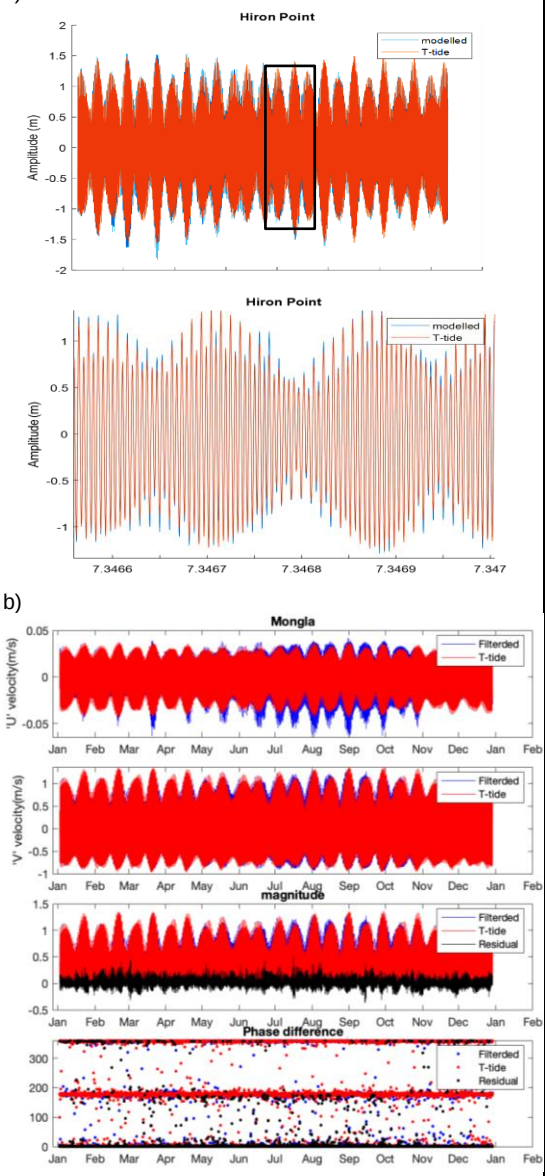

Figure 3.7: Outputs for T_tide a) water level series at HironPoint, and b) velocity time series data at Mongla station, for the analysis period of 2011. Where, Godin-filtered series (blue line), T_tide modelled time series (blue line) and residual series (black line)

4 Results

4.1 Analysing existing data

4.1.1 Water level

The existing measured WL level data from BWDB and BIWTA are plotted (Figure 4.1) to see the tidal range between the high tide and low tide. From figure 3.3, it is found that the tidal range in the Sibsa-Pussur (SP) system has been increasing since 1976.

The increase in tidal range leads to an increase in high waters. For the Hironpoint station (most seaward station), both the high tide and low tide are increasing (Figure 3.3a), but still, there is a clear indication of increasing the tidal range over time. For the Mongla and Rupsha stations (both are landward stations), the annual high water increased, and low water decreased (Figure 3.3b & 3.4). The increase in high water with the decrease in low water are the results of tidal amplification.

With that, to examine the shape of the tidal curve, one day of data was plotted for Hironpoint, Mongla and Rupsha stations during the dry and wet period of the year 2011 (Figure 4.2). The figures show that the tidal curve becomes increasingly asymmetric in the landward direction

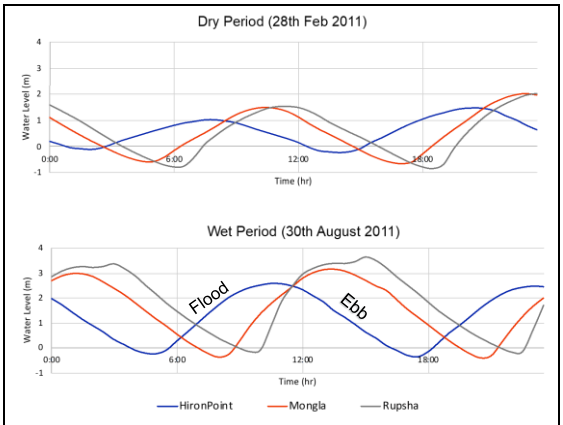

Figure 4.2: Single-day water level data at Hironpoint, Mongla and Rupsha stations during the dry and wet periods of the year.

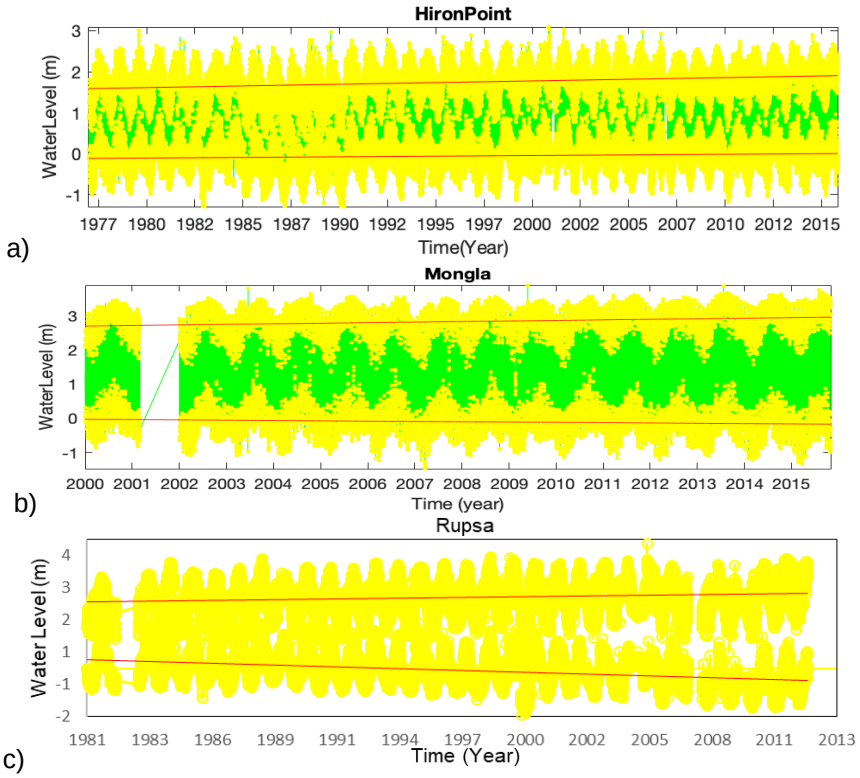

Figure 4.1: Observed water levels at a) HironPoint, b) Mongla, and c) Rupsha. The yellow dots are the highest and the lowest peak point of a day, and the red line is the trendline providing daily lowest and highest water levels.

4.1.2 River Characteristics

As mentioned earlier, 21 observation points (OPs) are taken in the Sibsa and Pussur river model. Among them, 12 OPs are in the Pussur system, and 08 OPs are in the Sibsa system. The Hironpoints OP is considered as common for both rivers. All these OPs are chosen on the thalweg of the river. Figure 4.3 shows the river depth and width illustrate from the model bathymetry of the corresponding OPs. Both the river's width is decreasing towards the landward direction, which means these rivers are converging. Considering river depth, Sibsa shows a slightly deeper channel than the Pussur. In both cases, river depth decreases except for a drop at 40km for Sibsa and a sudden rise at 45km for Pussur. The depth of the Pussur increases after around 93 km.

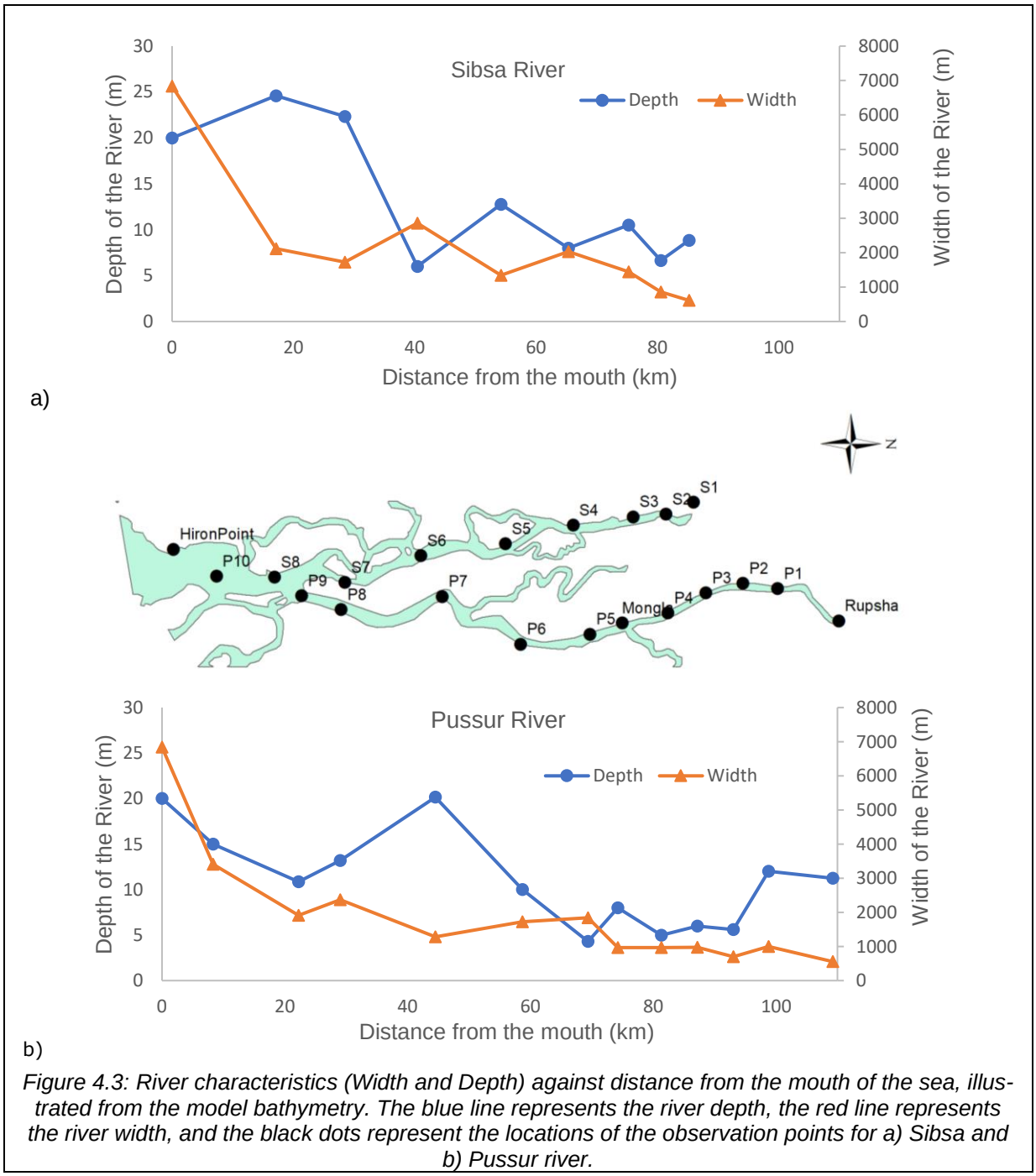

Figure 4.3: River characteristics (Width and Depth) against distance from the mouth of the sea, illustrated from the model bathymetry. The blue line represents the river depth, the red line represents the river width, and the black dots represent the locations of the observation points for a) Sibsa and b) Pussur river.

4.2 Asymmetry of the vertical tide

4.2.1 Spatial variation of tidal amplitudes

Like other semi-diurnal estuaries, tidal asymmetry in the Sibsa-Pussur (SP) estuary can be related to M2, S2, K1, O1, M4, M6, MS4, MSf, which are further analysed here. M2 is the most dominant tidal constituent in the SP system, followed by S2, K1, and MS4 (Figure 4.4 & 4.5). Besides that, M4 is also considered because it is the first harmonic of M2 and dominates in many estuaries. The tidal asymmetry can also be affected by the sixth-diurnal tide M6 in some, mainly semi-diurnal estuaries. Near the coast, the effects of the fortnightly tide MSf are limited compared with those of the main diurnal and semi-diurnal tides. Figure 4.4 shows how the amplitudes of these eight constituents enlarge in the landward direction. However, the enlargement rate is different in these two different rivers (Figure 4.5a & 4.5b). The geometric convergence and decreasing depth of the Sibsa and Pussur river (Figure 4.3) may lead to a gradual increase in tidal amplitudes towards the estuary's landward direction.

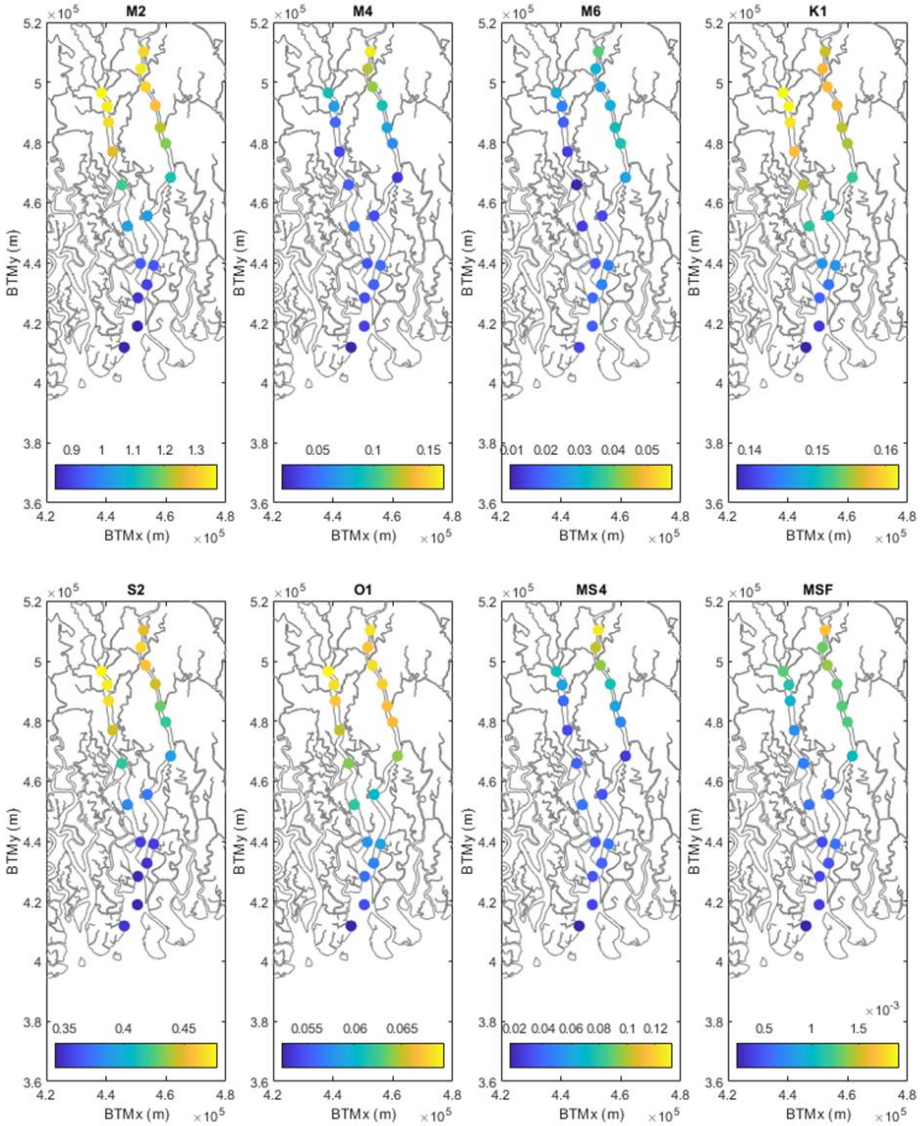

Figure 4.4: Spatial variation of the vertical tidal amplitudes (M2, M4, M6, K1, S2, O1, MS4 and MSf) for the year 2011 tidal analysis.

Focusing on the main diurnal constituents K1 and O1, the T_tide results show that the variations of the mean amplitudes are in the range 0.19–0.23 m and 0.05–0.08 m, respectively, among the different stations. The mean amplitudes of the main semi-diurnal constituents M2 and S2 range between 0.8–1.35m and 0.28m – 0.4m, respectively (Figure 4.5). The largest amplitudes are found at the stations around the rivers' landward direction, where the poldered areas start (Figure 3.2). The S2 amplitude is about one-third of the M2 amplitude. The narrowing of the rivers also enhances the overtides and compound tides, such as M4, MS4 and M6. The peak values of M4, MS4 and M6 amplitudes are found 0.17m, 0.12m and 0.06m, respectively (Figure 4.5). There is also a landward increase of the MSf amplitude throughout the estuary. However, compared to other constitutes, the contribution from the MSf is relatively small to the tide.

Two main channels are identified within the SP estuary: the Sibsa channel and the Pussur channel. For these two channels, the along channel variations of the mean tidal amplitudes of eight main constituents are shown in Figure 4.5a and 4.5b. M2 is the most dominant tides in both cases, followed by the S2, K1, MS4, M4, O1, M6 and MSf. M2 has a similar amplitude until the bifurcation point (about 13 km from the mouth of the ocean) of the two rivers; from that point onward, the trends increase. At the point of around 93km of the Pussur channel, there was a downward trend for the M2 and S1 amplitudes. The possible reason for this change is probably the presence of interconnected channels at that point (Figure 3.2). This may cause the scouring and increase the depth (Figure 4.3), lead to decreasing M2 and increment of M4.

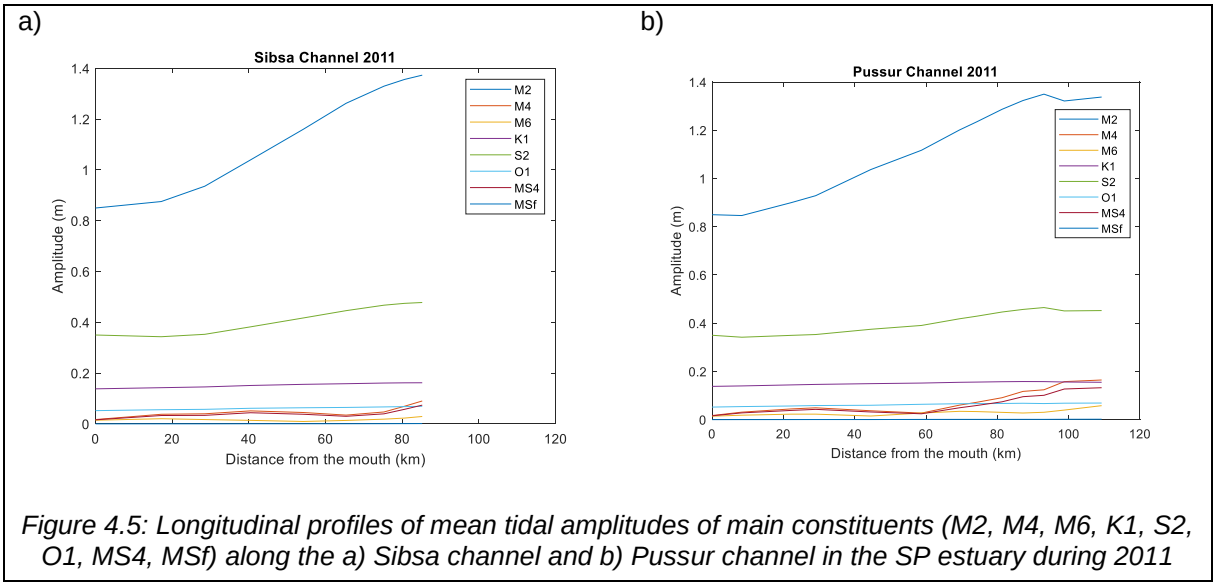

Figure 4.5: Longitudinal profiles of mean tidal amplitudes of main constituents (M2, M4, M6, K1, S2, O1, MS4, MSf) along the a) Sibsa channel and b) Pussur channel in the SP estuary during 2011

4.2.2 Temporal Variation of tidal Amplitude

From the year 1978 to 2011, four different years (1978, 1988, 2000, and 2011) choose to run the model for mimicking the temporal variation of over 33 years. The choice of the year depends on data availability and hydrological characteristics. The year 1978 is the earliest available data year, 1988 is the most flooded year, 2000 is the driest year, and 2011 is the latest available data and model validating year.

Figure 4.6 shows the model predictions of amplitude ratios along the Sibsa and Pussur channel between 1978 and 2011. Figure 4.6a and 4.6b show that the Pussur channel's tidal asymmetry is more robust than in the Sibsa channel. There is a slight drop at 65km for the Sibsa channel and around 60 km for the Pussur channel. Among the years, 1988 shows the strongest tidal asymmetry, followed by the year 2000, 1978, and 2011 for the Sibsa channel, and 1978, 1988, and 2011 for the Pussur channel.

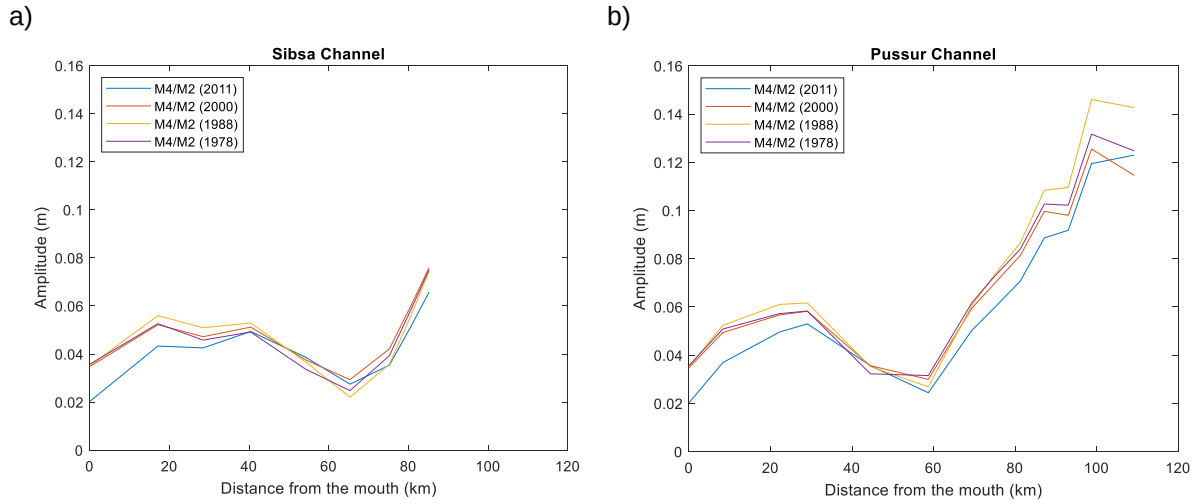

Figure 4.6: The evolution of the amplitude ratio of the M2 and M4 (a & b) tidal constituent for the asymmetry of the vertical tide, derived from the model, along the Sibsa-Pussur channel between1978 and 2011.

1

4.3 Asymmetry of the horizontal tide

4.3.1 Spatial variation of tidal current amplitude

The same observation points are used in the model for analysing the asymmetry of the horizontal tide, as used in the asymmetry of the vertical tide. Time-series predictions (every 30min) of tidal velocities are computed for each observation point in the model. The time series are harmonically analysed to derive the contribution of the most critical tidal constituents. The observation points' location within the channel section influenced the results significantly since velocities were highly affected by the local bathymetry. Therefore, the trend between the asymmetry of the vertical tide and asymmetry of the horizontal tide is different from each other. Figure 4.7 shows the spatial variation of tidal currents for different tidal constituents during the year 2011.

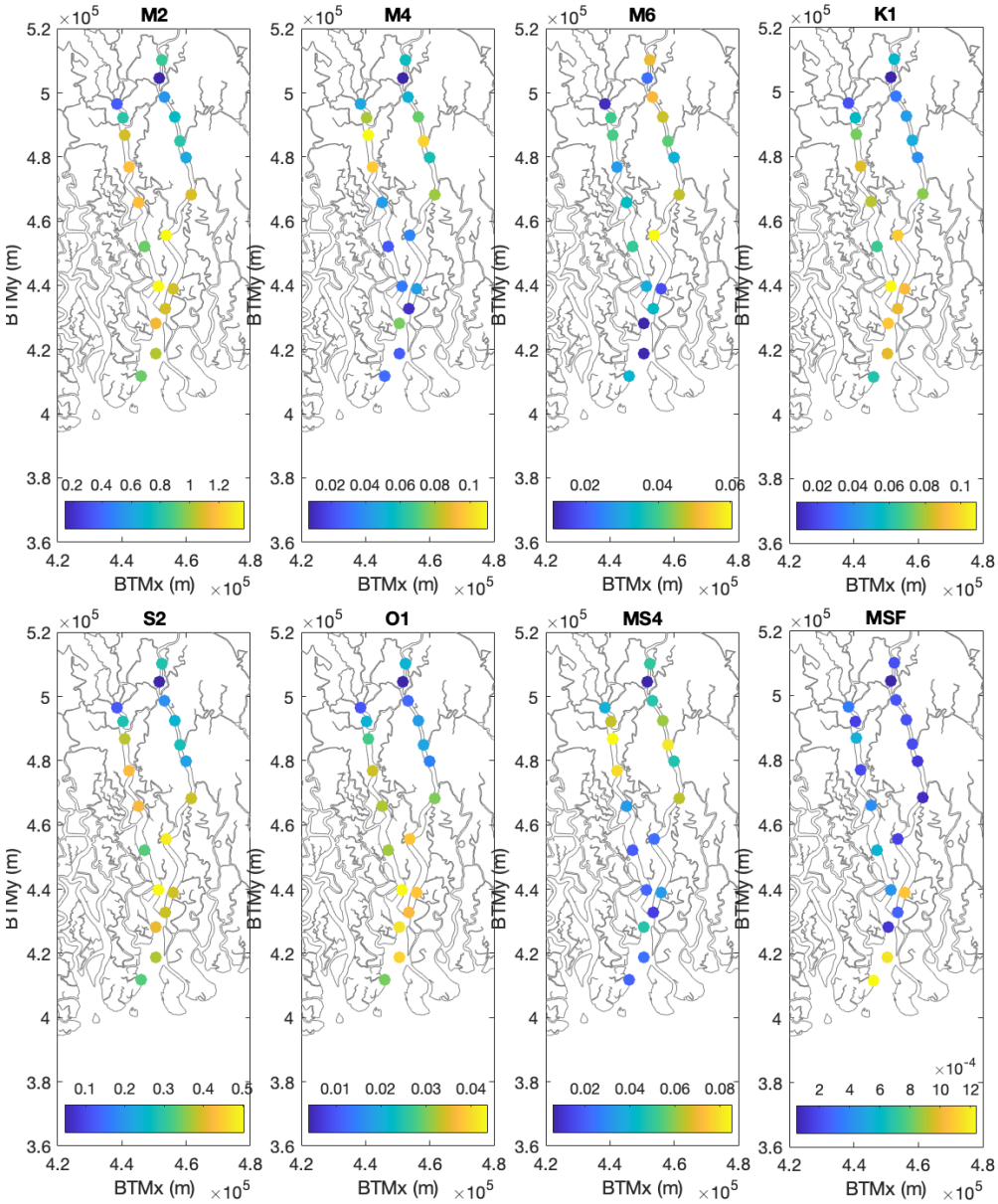

Figure 4.7: Spatial variation of the horizontal tidal current amplitudes (M2, M4, M6, K1, S2, O1, MS4 and MSf) for the year 2011 tidal analysis.

Though there are no observable trends found in horizontal tidal constituents like the vertical one, M2 is the most dominating tidal constituents, followed by the S2, K1, and M4 (Figure 4.8). Some other overtides like O1 and M6 are quite the same throughout both channels (Figure 4.8a & 4.8b). In some places, MS4 is more dominating over these two overtides (O1, M6). Here, MSf is less significant for the horizontal tide as well. From figure 4.8a, it is found that for the Sibsa channel, there is an increasing trend for M2, S2, and K1 tidal current amplitudes until the point at 30km. Afterwards, there is a slight drop, then again increase until 65km. After that, there is a considerable drop found for these three tidal constituents. The trend seems quite similar to the depth of the Sibsa river (Figure 4.3). On the other side, in the Pussur channel same three tidal constituents follow the increasing trend till point 45km (Figure 4.8b). Afterwards, two visible drops are found around at 65km and 93km in the Pussur channel. All these abrupt changes of tidal currents can be related to the major bathymetry changes or the diversion of the river water through different interconnected channels.

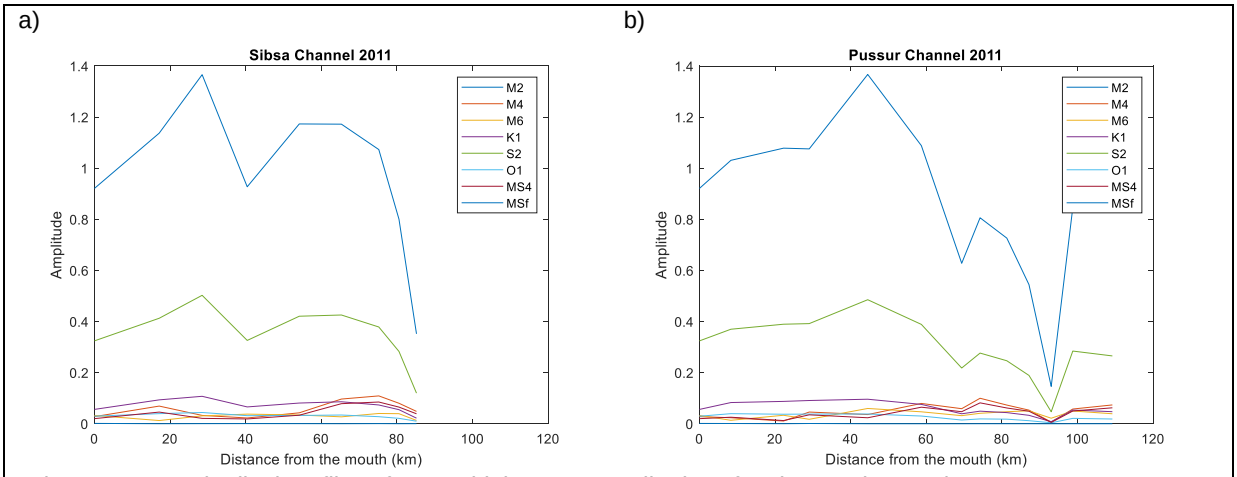

Figure 4.8: Longitudinal profiles of mean tidal current amplitudes of main constituents (M2, M4, M6, K1, S2, O1, MS4, MSf) along the a) Sibsa channel and b) Pussur channel in the SP estuary during 2011

4.3.2 Temporal variation of tidal currents

Like vertical tidal analysis, the same four years are taken for analysing the temporal variation of the horizontal tidal currents. Figure 4.9 shows the temporal variation for both the river Sibsa and Pussur. In all four cases, the year 1988 shows the most distorted tide, followed by the year 1978, 2000, and 2011 for the M4/M2 ratio (figure 4.9 a & b)

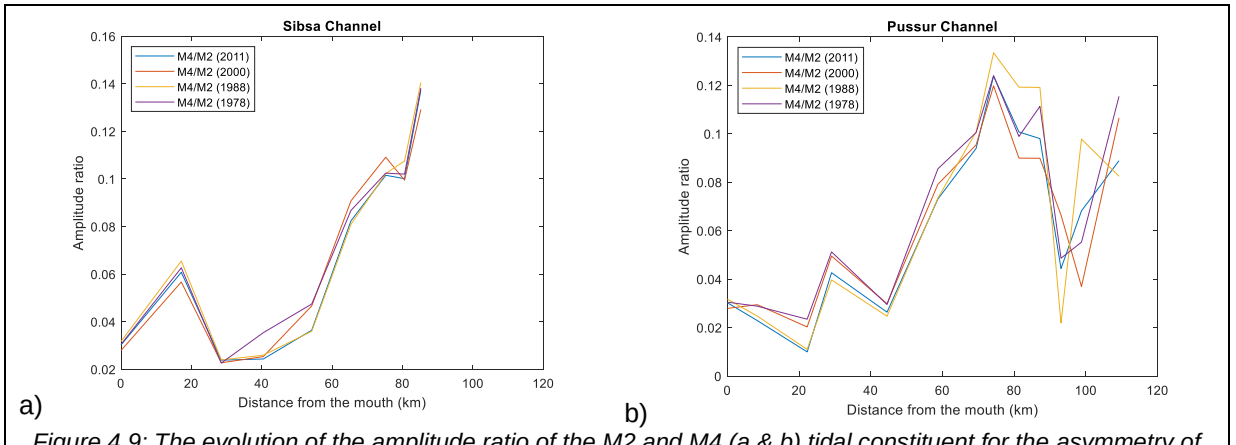

Figure 4.9: The evolution of the amplitude ratio of the M2 and M4 (a & b) tidal constituent for the asymmetry of the horizontal tide, derived from the model, along the Sibsa-Pussur channel between 1978 and 2011.

4.4 Nature of the Tidal Asymmetry

Whether the system is flood dominant or ebb dominant, this can be determined from the calculations of phase difference ($2\varphi_2 - \varphi_4$) (see chapter two for detail). In the case of asymmetry of the horizontal tide, a system is called flood dominant when the phase difference is lies between 0°- 90° & 270°- 360°. From 90°- 270° represent the system as ebb dominant. If the phase difference is close to 90° or 270° (-90°), then the system is known as the symmetric tide. So more far from these two points will represent more asymmetric tide. For the SP estuary, phase differences are calculated from the tidal analysis of horizontal tide (Figure 4.10) and vertical tide (Figure 4.11) for the year 1978, 1988, 2000 and 2011.

Peak current asymmetry

Figure 4.10 shows the peak current asymmetry of both the Sibsa (dotted line) and Pussur (solid line) river along with the longitudinal profile and four different years of temporal variation. In the Sibsa channel, the temporal variations of the tidal asymmetry are not that much, except for the first point and at 30km (Figure 4.10). However, the spatial variations are significant. Initially, it seems to be ebb dominant till 30 km, then goes close to the flood dominant to symmetric. After 80 km, the asymmetry becoming maximum flood dominant.

On the other side, in the Pussur channel, there are some temporal variations along the river at 23 km, 45km and 93km (Figure 4.10). Where from 0 to 40km, recent years show more close to the ebb dominance. However, the rest of the river shows flood dominance. The asymmetry towards the longitudinal profile of the Sibsa river also shows flood dominant in most of the points (Figure 4.10).

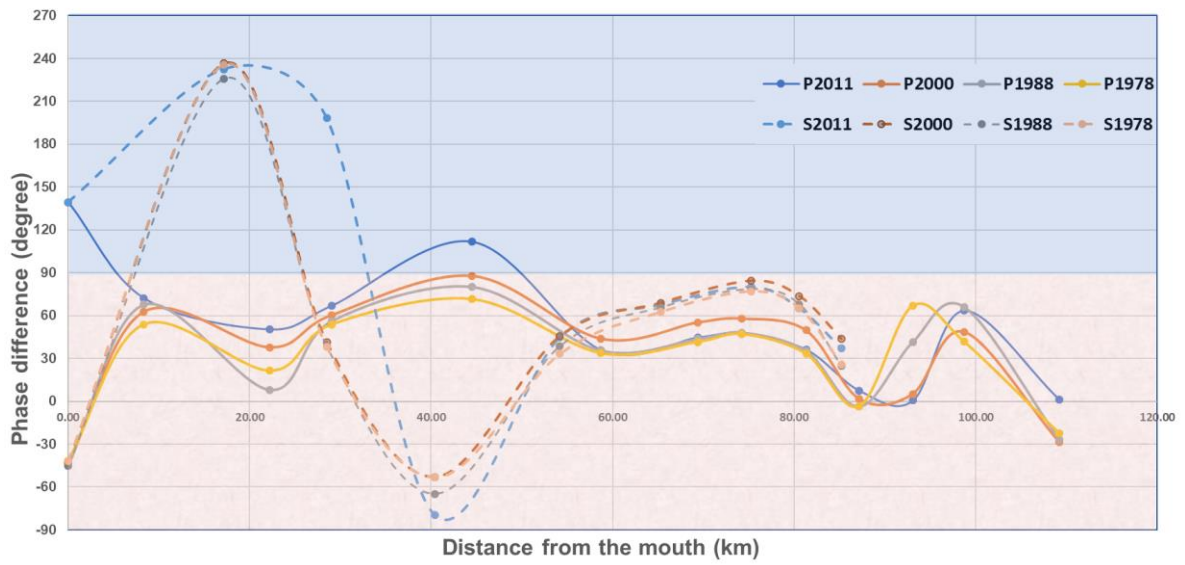

Figure 4.10: Comparison of asymmetry of the horizontal tide between the Sibsa and the Pussur channel. The blue and red shaded area represents the ebb and flood dominant zone, respectively. The dotted line represents the Sibsa channel, and the solid line represents the Pussur channel.

1

Tidal duration asymmetry

From figure 4.11, it is found that the Sibsa channel shows more symmetrical behaviour considering the tidal duration asymmetry. In contrast, the Pussur is becoming more flood dominant over time and toward the landward direction. The central part of the Sibsa river (from 30 to 60 km) is symmetric or slightly ebb dominant; afterwards, it becomes flood dominant. Whereas the Pussur behaves differently, it shows maximum flood dominant asymmetry in the central (at around 60km). Afterwards, it stayed at maximum flood dominance, almost throughout the rest of the channel. From 0 to around 40km, Pussur behaves the same as Sibsa, becoming symmetric from the flood dominance asymmetry.

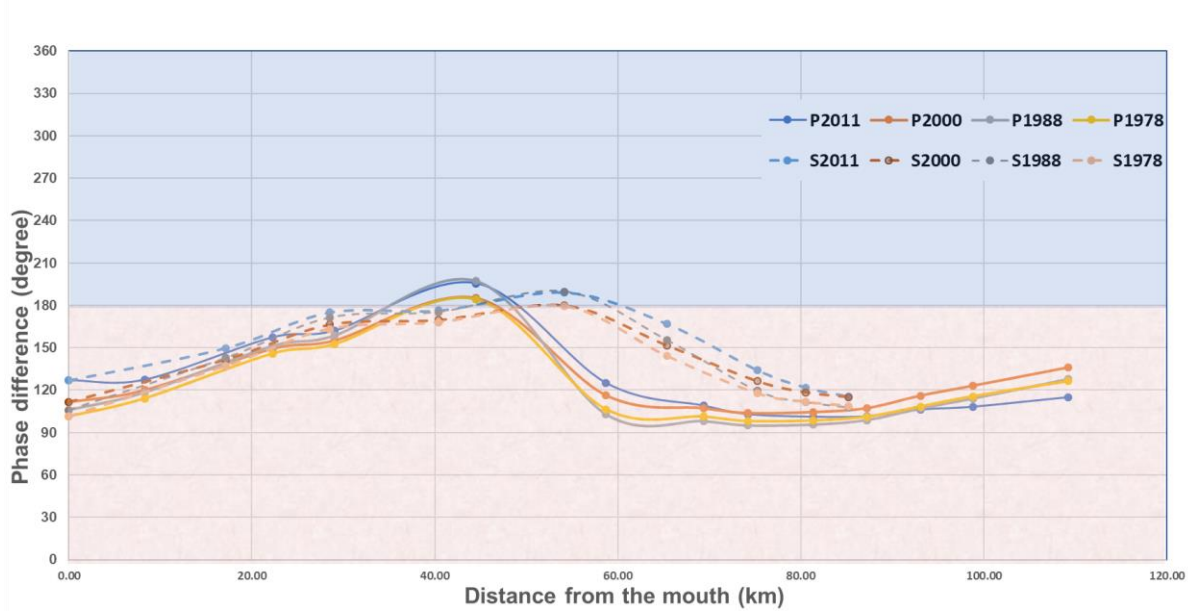

Figure 4.11: Comparison of asymmetry of the vertical tide between the Sibsa and the Pussur channel. The blue and red shaded area represents the ebb and flood dominant zone, respectively. The dotted line represents the Sibsa channel, and the solid line represents the Pussur channel.

4.5 Relation with the upstream discharge

The nonstationary harmonic analysis (NS_tide; developed by Matte et al., 2013) is applied to see the impact of river discharge on tidal asymmetry.

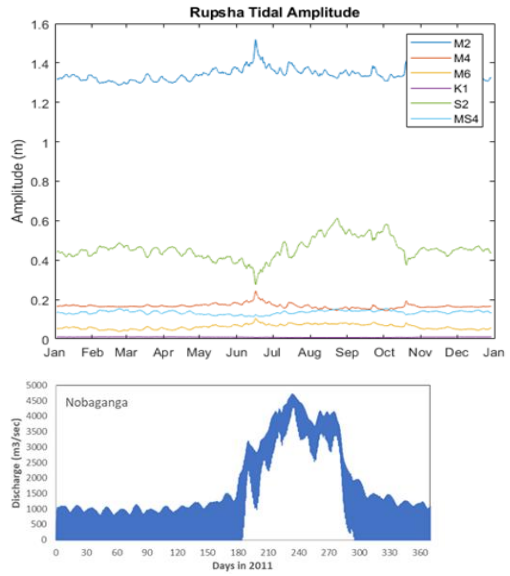

Figure 4.12: Impact of discharge on different tidal constituents.

The outcomes show a direct relation with the discharge and M2, M4 amplitude of the SP system. When there is a higher discharge available in the system, the M2 and M4 amplitudes are also at their peak (Figure 4.12). With that, two hypothetical scenarios have been developed (1.5Q and 2Q) considering no Farakka barrage on upstream of the river. All the previously mentioned tidal analysis are done and compared with the year 2011 (referred to as 1Q in figure 4.13).

Figure 4.13 shows that if there is no discharge reduction present in the system, then the Sibsa channel's tidal asymmetry will not change that much. However, the Pussur channel will become symmetrical from flood dominating asymmetric tide. This means the Pussur channel is more sensitive to the upstream river discharge.

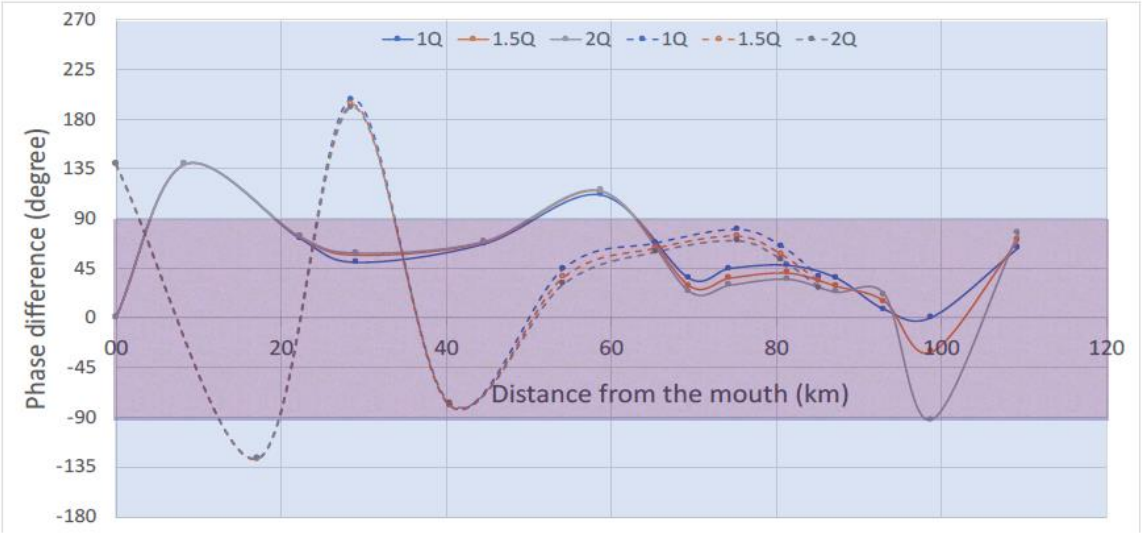

Figure 4.13: Changes in tidal asymmetry considering the higher discharge coming from the upstream river. The blue and red shaded area represents the ebb and flood dominant zone, respectively. The dotted line represents the Sibsa channel, and the solid line represents the Pussur channel.

5 Discussion

5.1 Tidal asymmetry in the Sibsa-Pussur estuary

Among various tidal asymmetry types, tidal asymmetry of the vertical tide (tidal duration asymmetry) and tidal asymmetry of the horizontal tide (peak current asymmetry) are determined here. The vertical tide's amplitude ratio shows that significant changes are around 65km at the Sibsa channel and 58km at the Pussur channel (Figure 4.6). Figure 4.5 shows that M2 tide is amplified in both channels, but there is a drop in amplitude ration (M4/M2). This means the M2 is suddenly increased in those points. From the study area map (Figure 3.2), it is visible that there is an interconnected river at those points, which possibly influence the M2 amplitudes.

The horizontal tide's amplitude ratio demonstrates many anomalies in both the Sibsa and Pussur channel (Figure 4.9). The M2 tides also show the same kind of peculiarity (Figure 4.8). The river bathymetry influences the horizontal tide (tidal current) a lot. That is why any small changes in bathymetry have an enormous impact on it. However, the morphological changes did not consider during the model run, but the existing bathymetry was developed based on field measurement, considering depth, width convergence, or divergence of the river (Figure 4.3). So, in the existing bathymetry, there are some influences of the polderization or the dredging operation. Figure 4.8 shows a massive drop in M2 amplitude at around 85 km for the Sibsa channel and around 93 km for the Pussur channel, from where the poldered areas are started for the respective rivers, which causes the width convergence (Figure 3.2 & 4.3).

The model used here only considered the intertidal area until the point where no polder is present. After that, the grid only covers the river (Figure 3.3). This means from the poldered point, there is no chance for river water to overtop the embankment, which leads to amplify the water level and exaggerated the flood dominance at those points. Among these two rivers, the Pussur shows more asymmetry than the Sibsa river (Figure 4.10 & 4.11), possibly because of the combination of different anthropogenic work such as dredging.

It is also found that both the horizontal tide and vertical tide are becoming flood dominant for both the rivers (Sibsa and Pussur) (Figure 4.10 & 4.11). The relative phase differences of vertical tides show smoother outliers, whereas the relative phase differences of horizontal tides show peculiar outliers over the landward direction. Because the horizontal tides (tidal currents) are far more sensitive to river geometry and river discharge than the vertical tide (tidal water level). In both cases, the phase differences are becoming symmetric initially (landward direction), going through the Sundarbans region. This region is represented as less influenced by anthropogenic work (no presence of polder). After entering the poldered area or dredged influenced area, it becomes the maximum flood dominant asymmetry (Figure 4.10 & 4.11), representing an apparent influence of anthropogenic work on these two rivers.

Among the Sibsa and Pussur river, Sibsa shows symmetric till the 60km of distance from the ocean mouth. Then it is gradually becoming flood dominant. On the contrary, the Pussur river becomes flood dominant after 45 km and reached maximum flood dominant asymmetry

at 60 km. From 60 to 90 km, it stayed at the maximum flood dominant asymmetry phase, where in reality, all the anthropogenic activities (the mongla seaport, dredging operation, polderization) are present. So, possibly the anthropogenic activity influences the Sibsa river to become more flood dominant asymmetry than the Sibsa river. Due to the Mongla seaport, the Pussur channel is always going thorough the dredging operation for maintaining the navigability for the ships. Still, the depth of Pussur is lower than the Sibsa river (Figure 3.3 & 4.3), which indicates that the Pussur is more affected by the sedimentation problem than the Sibsa. Though in this study, no morphological changes are considered during the model run, but in future, further study considering dynamic morphology will help to understand the impact of dredging work more accurately.

5.2 Impact of tidal asymmetry on sediment transport.

As mentioned before, the SP estuary is facing sedimentation problems. Naturally, this system is connected to lots of peripheral rivers. However, in recent time these peripheral rivers are rapidly filling in and/or losing their navigability. Wilson et al., (2017) show that 16 km of channels still annually close over the whole GBM delta, and 98% of this change is happening in the poldered area where only 2% closing occurred in the natural system (Sundarbans area).

The results and previous discussion show that most of the places of the SP estuary become flood dominant over time. Hoitink et al., (2017) show that in tide dominant delta, due to the flood dominance tidal asymmetry, inland sediment transport dominants over the sediment with the river discharge and tide enhance seaward sediments, which causes the sediment accumulation in deltas. Bricheno et al., (2016) classified the western part of the GBM delta as a Macro tidal (tidal range > 4 m) area. So, as a tide dominating delta, this sediment transport phenomenon due to flood dominance asymmetry can cause the SP estuary sedimentation problem. On the contrary, ebb dominance can causes erosion as well.

The depth of the Sibsa and Pussur channel has an enormous impact on tidal propagation and its velocity. Between the Sibsa and Pussur channel, Sibsa is deeper than the Pussur (Figure: 3.3 & 4.3). During both ebb and flood current, the Sibsa channel velocity is much higher than the Pussur channel velocity (Figure 5.1). According to the sediment transport theory, sediment will transport from the sea to the land during the flood current, and the opposite phenomenon will happen during the ebb current. Now, if both the currents become the same, then an equilibrium situation will be present there. This means no sedimentation or erosion will occur. However, any distortion between these two current will cause either sedimentation or erosion. If the flood current shows more velocity than the ebb current, then the relatively low velocity allows them to settle down the sediment and causes sedimentation. The opposite phenomena will cause erosion.

In the SP system, the flood current shows more velocity than the ebb current (Figure 5.1), which causes the sedimentation, except for some portion of the Sibsa river (around 20 km), where ebb dominance is present (Figure 4.10) and can cause erosion. However, the overall SP estuary faces the sedimentation problem. It changes the SP estuary's morphology, which leads to the flood dominant tidal asymmetry. Again, this tidal asymmetry causes the sedimentation problem. So, this whole positive feedback loop makes the problem even worse.

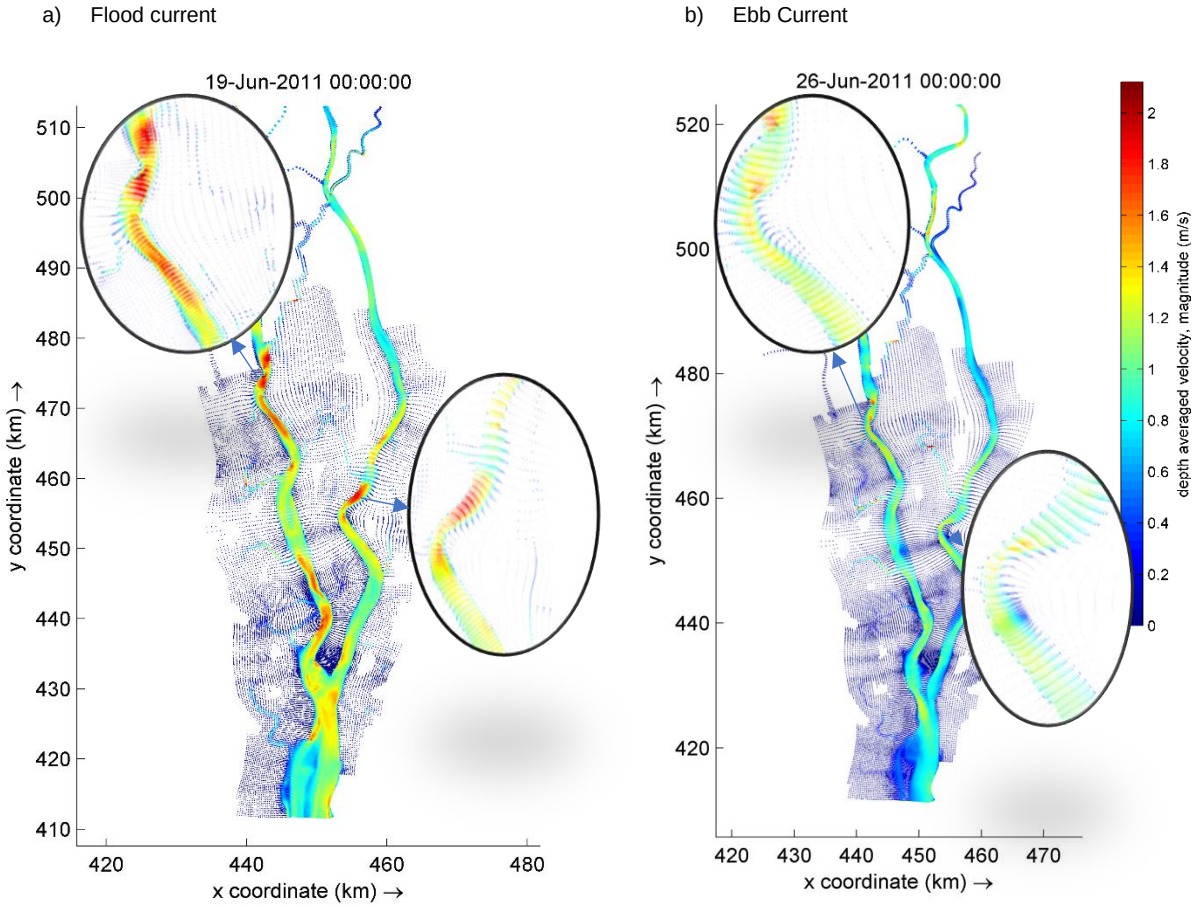

Figure 5.1: Velocity profile of SP estuary during the a) flood and b) ebb current flow.

5.3 Impact of river discharges on tidal duration asymmetry.

Diversion of water by the Farakka barrage reduce the upstream river discharge of the SP estuary. So, it is important to see the impact of river discharge on the system's tidal asymmetry. From the result of hypothetical increased discharged, it is found that both the Sibsa and Pussur channel has become more symmetric than the present time (Figure 4.13). This means that closure of the Farraka barrage decreased discharge towards the SP system, resulting in an increase in flood dominant conditions, which can lead to an increased import of sediment and may contribute to the observed increase in channel siltation in the SP system.

The temporal variation of tidal asymmetry (both vertical and horizontal) also represents the impact of discharge on the tidal asymmetry. As mentioned earlier, 1988 was the wettest year, so it represented the high discharge year. On the other side, 2000 was a comparatively dry year, which means less discharge comes from upstream. From the results (Figure 4.10 & 4.11), it is difficult to differentiate between 1988 and 2000. However, with higher discharge, the year 1988 shows weaker flood asymmetry than the year 2000.

6 Conclusions

A harmonic analysis method is applied to examine the spatiotemporal evolution of tidal asymmetry in the Sibsa-Pussur (SP) estuary of the GBM delta. The required data is generated using a hydrodynamic model (Delft-3D) for the year 1978, 1988, 2000 and 2011. The eight main tidal constituents (M2, M4, M6, K1, S2, O1, MS4, MSf) are considered for data analysis. The tidal duration asymmetry (as tidal asymmetry of the vertical tide) and peak current asymmetry (as tidal asymmetry of the horizontal tide) are determined here. The results quantify the tidal asymmetry based on the amplitude ratio (a_{M4}/a_{M2}) and phase difference ($2\theta_{M2} - \theta_{M4}$). The morphological effects are assessed based on the response of tidal asymmetry to varying river discharge and downstream boundary conditions (changing WL), with the following main findings:

1) Despite some anomalies in the peak current asymmetry, most parts of the Sibsa-Pussur system are flood dominant. Tidal asymmetry changes are slightly symmetric, followed by maximum flood dominant asymmetry towards the delta's landward direction under the substantial effect of nonlinear interactions. The M2 and M4 amplitudes are found more dominant among the other semi-diurnal tides and overtides, respectively. Temporal variation in the tidal asymmetry is found very little, considering the hydrodynamical changes only.
2) Compare to the Sibsa; the Pussur channel is more flood dominant. The Sibsa channel shows more symmetrical behaviours, whereas the Pussur channel mostly shows maximum flood dominant asymmetry. The influence of anthropogenic activities on the Pussur system is more significant than the Sibsa system.
3) Changing the river discharge plays a significant role in determining the tidal regime of the SP estuary. This effect also has seasonal variability. With increasing discharge, flood dominant tidal asymmetry is weaker, and the system becomes more symmetric than the present reduced discharge situation.

Acknowledgements

I would like to start by giving thanks to the Almighty ALLAH for giving me the ability to complete this research work. With this thesis report, I will end my two-year journey of Masters at Wageningen University and Research. It would not have been possible to come to this stage without the help and support of the kind people around me and the organisations with their financial support. Therefore I would like to take this opportunity to express my sincere gratitude to honour their contributions.

First and foremost, I would like to extend my sincere gratitude to my supervisors, Ton Hoitink and Reinier Schrijvershof, for giving me the opportunity to do my research and allow me to be a part of the Deltas out of Shape project. I am greatly indebted to them for their guidance, constructive feedback and continuous encouragement throughout the project. I want to express my special gratitude and appreciation for Reinier for his profound technical support on MATLAB programming and modelling in Delft3D.

Besides, I want to thank Sjoukje, Kris, and again Reinier to teach me some life lessons and all the crew members for their support during the field visit. I would also like to thank Bas van Maren from Deltares for permitting me to use the Sibsa-Pussur model in my study. The entire HWM chair group from Wageningen University, including the other MSc thesis students, are thanked for their thoughts and constructive feedback during the thesis rings and any other moments.

I would like to thank Bangladesh's prime minister fellowship program for opening the door for me to conduct my higher study in the Netherlands. Thanks also to the Shere-Bangla Agricultural University, Dhaka, to allow me the official leave.

Finally, I want to thank my family for supporting me, especially my wife, Taznin, for staying alongside me throughout this journey.

References

Angamuthu, B., Darby, S. E. & Nicholls, R. J. (2018). Impacts of natural and human drivers on the multi-decadal morphological evolution of tidally-influenced deltas. *Proceedings of the Royal Society A: Mathematical, Physical and Engineering Sciences*, *474*(2219), 20180396. https://doi.org/10.1098/rspa.2018.0396

Auerbach, L. W., Goodbred, S. L., Mondal, D. R., Wilson, C. A., Ahmed, K. R., Roy, K., Steckler, M. S., Small, C., Gilligan, J. M. & Ackerly, B. A. (2015). Flood risk of natural and embanked landscapes on the Ganges-Brahmaputra tidal delta plain. *Nature Climate Change*, *5*(2), 153–157. https://doi.org/10.1038/nclimate2472

Bomer, E. J., Wilson, C. A. & Datta, D. K. (2019). An integrated approach for constraining depositional zones in a tide-influenced river: Insights from the Gorai River, Southwest Bangladesh. *Water (Switzerland)*, *11*(10), 2047. https://doi.org/10.3390/w11102047

Bricheno, L. M., Wolf, J. & Islam, S. (2016). Tidal intrusion within a mega delta: An unstructured grid modelling approach. *Estuarine, Coastal and Shelf Science*, *182*, 12–26. https://doi.org/10.1016/j.ecss.2016.09.014

BWDB. (2013). *Final Report On Environmental Impact Assessment (EIA) CEIP-I* (Issue January). https://www.bwdb.gov.bd/archive/pdf/284.pdf

Calero Quesada, M. C., García-Lafuente, J., Garel, E., Delgado Cabello, J., Martins, F. & Moreno-Navas, J. (2019). Effects of tidal and river discharge forcings on tidal propagation along the Guadiana Estuary. In *Journal of Sea Research* (Vol. 146, pp. 1–13). Elsevier B.V. https://doi.org/10.1016/j.seares.2019.01.006

De Swart, H. E. & Zimmerman, J. T. F. (2009). Morphodynamics of tidal inlet systems. *Annual Review of Fluid Mechanics*, *41*, 203–229.

Deltares. (2014). *3D/2D modelling suite for integral water solutions: Hydro-Morphodynamics*. 710.

Dronkers, J. (1986). Tidal asymmetry and estuarine morphology. *Netherlands Journal of Sea Research*, *20*(2–3), 117–131.

Friedrichs, C. T. & Aubrey, D. G. (1988). Non-linear tidal distortion in shallow well-mixed estuaries: a synthesis. *Estuarine, Coastal and Shelf Science*, *27*(5), 521–545. https://doi.org/10.1016/0272-7714(88)90082-0

Gallo, M. N. & Vinzon, S. B. (2005). Generation of overtides and compound tides in Amazon estuary. *Ocean Dynamics*, *55*(5–6), 441–448.

Godin, G. (1972). The analysis of tides. In *Univ. of Toronto Press,*. https://doi.org/10.1016/0025-3227(73)90070-4

Gong, W., Schuttelaars, H. & Zhang, H. (2016). Tidal asymmetry in a funnel-shaped estuary with mixed semidiurnal tides. *Ocean Dynamics*, *66*(5), 637–658. https://doi.org/10.1007/s10236-016-0943-1

Groen, P. (1967). On the residual transport of suspended matter by an alternating tidal current. *Netherlands Journal of Sea Research*, *3*(4), 564–574.

Guo, L., Van Der Wegen, M., Roelvin, J. A. & He, Q. (2014). The role of river flow and tidal asymmetry on 1-D estuarine morphodynamics. *Journal of Geophysical Research F: Earth Surface*, *119*(11), 2315–2334. https://doi.org/10.1002/2014JF003110

Guo, Leicheng, Wang, Z. B., Townend, I. & He, Q. (2019). Quantification of Tidal Asymmetry and Its Nonstationary Variations. *Journal of Geophysical Research: Oceans*, *124*(1), 773–787. https://doi.org/https://doi.org/10.1029/2018JC014372

Guo, S., Sun, J., Zhao, Q., Feng, Y., Huang, D. & Liu, S. (2016). Sinking rates of phytoplankton in the Changjiang (Yangtze River) estuary: A comparative study between Prorocentrum dentatum and Skeletonema dorhnii bloom. *Journal of Marine Systems*, *154*, 5–14. https://doi.org/10.1016/j.jmarsys.2015.07.003

Hoitink, A. J. F., Hoekstra, P., Van Maren, D. S. & Hoitink, C. : (2003). Flow asymmetry associated with astronomical tides: Implications for the residual transport of sediment. *J. Geophys. Res*, *108*(C10), 3315. https://doi.org/10.1029/2002JC001539

Hoitink, A. J. F., Wang, Z. B., Vermeulen, B., Huismans, Y. & Kästner, K. (2017). Tidal controls on river delta morphology. In *Nature Geoscience* (Vol. 10, Issue 9, pp. 637–645). Nature Publishing Group. https://doi.org/10.1038/ngeo3000

Islam, M. A. & Haider, M. Z. (2016). Performance assessment of Mongla seaport in Bangladesh. *International Journal of Transportation Engineering and Technology*, *2.2*(2), 15. https://doi.org/10.11648/j.ijtet.20160202.11

Jiang, A. W., Ranasinghe, R., Cowell, P. & Savioli, J. C. (2011). Tidal asymmetry of a shallow, well-mixed estuary and the implications on net sediment transport: A numerical modelling study. *Australian Journal of Civil Engineering*, *9*(1), 1–18. https://doi.org/10.1080/14488353.2011.11463962

Kennish, M. J. (2016). *Encyclopedia of Estuaries (Encyclopedia of Earth Sciences Series).* Springer.

Lanzoni, S. & Seminara, G. (1998). On tide propagation in convergent estuaries. *Journal of Geophysical Research: Oceans*, *103*(C13), 30793–30812. https://doi.org/10.1029/1998jc900015

Li, K., Liu, X., Zhao, X. & Guo, W. (2010). Effects of reclamation projects on marine ecological environment in Tianjin Harbor Industrial Zone. *Procedia Environmental Sciences*, *2*, 792–799. https://doi.org/10.1016/j.proenv.2010.10.090

Matte, P., Jay, D. A. & Zaron, E. D. (2013). Adaptation of classical tidal harmonic analysis to nonstationary tides, with application to river tides. *Journal of Atmospheric and Oceanic Technology*, *30*(3), 569–589. https://doi.org/10.1175/JTECH-D-12-00016.1

Matte, P., Secretan, Y. & Morin, J. (2014). Temporal and spatial variability of tidal-fluvial dynamics in the St. Lawrence fluvial estuary: An application of nonstationary tidal harmonic analysis. *Journal of Geophysical Research C: Oceans*, *119*(9), 5724–5744. https://doi.org/10.1002/2014JC009791

Mirza, M. M. Q. (2004). The Ganges Water Diversion: Environmental Effects and Implications --- An Introduction. In M. M. Q. Mirza (Ed.), *The Ganges Water Diversion: Environmental Effects and Implications* (pp. 1–12). Springer Netherlands. https://doi.org/10.1007/978-1-4020-2792-5_1

Neill, S. P. & Hashemi, M. R. (2018). Chapter 10 - Other Aspects of Ocean Renewable Energy. In S. P. Neill & M. R. B. T.-F. of O. R. E. Hashemi (Eds.), *E-Business Solutions* (pp. 271–309). Academic Press. https://doi.org/https://doi.org/10.1016/B978-0-12-810448-4.00010-0

Nidzieko, N. J. (2010). Tidal asymmetry in estuaries with mixed semidiurnal/diurnal tides. *Journal of Geophysical Research*, *115*(C8), C08006. https://doi.org/10.1029/2009JC005864

Parker, B. (2016). Tidal hydrodynamics. In *Encyclopedia of Earth Sciences Series* (pp. 686–700). https://doi.org/10.1007/978-94-017-8801-4_115

Pawlowicz, R., Beardsley, B. & Lentz, S. (2002). Classical tidal harmonic analysis including error estimates in MATLAB using TDE. *Computers and Geosciences*, *28*(8), 929–937. https://doi.org/10.1016/S0098-3004(02)00013-4

Pethick, J. & Orford, J. D. (2013). Rapid rise in effective sea-level in southwest Bangladesh: Its causes and contemporary rates. *Global and Planetary Change*, *111*, 237–245. https://doi.org/10.1016/j.gloplacha.2013.09.019

Piano, M., Neill, S. P., Lewis, M. J., Robins, P. E., Hashemi, M. R., Davies, A. G., Ward, S. L. & Roberts, M. J. (2017). Tidal stream resource assessment uncertainty due to flow asymmetry and turbine yaw misalignment. *Renewable Energy*, *114*, 1363–1375. https://doi.org/https://doi.org/10.1016/j.renene.2017.05.023

Postma, H. (1961). Transport and accumulation of suspended matter in the Dutch Wadden Sea. *Netherlands Journal of Sea Research*, *1*(1–2), 148–190.

Rahman, M., Dustegir, M., Karim, R., Haque, A., Nicholls, R. J., Darby, S. E., Nakagawa, H., Hossain, M., Dunn, F. E. & Akter, M. (2018). Recent sediment flux to the Ganges-Brahmaputra-Meghna delta system. *Science of the Total Environment*, *643*, 1054–1064. https://doi.org/10.1016/j.scitotenv.2018.06.147

Rahman, M. Z., Beg, M. N. A. & Khan, Z. H. (2014). Sediment budget of Meghna Estuary. *Technical Journal River Research Institute*, *12*(1), 106–118. https://doi.org/10.5281/ZENODO.3351639

Rahman, Md Mahbubur & Rahaman, M. M. (2018). Impacts of Farakka barrage on hydrological flow of Ganges river and environment in Bangladesh. *Sustainable Water Resources Management*, *4*(4), 767–780. https://doi.org/10.1007/s40899-017-0163-y

Rahman, Md Motiur & Ali, M. S. (2018). Potential causes of navigation problem in Pussur river and interventions for navigation enhancement. *4th International Conference on Civil Engineering for Sustainable Development (ICCESD-2018)*.

Ranasinghe, R. & Pattiaratchi, C. (2000). Tidal inlet velocity asymmetry in diurnal regimes. *Continental Shelf Research*, *20*(17), 2347–2366. https://doi.org/10.1016/S0278-4343(99)00064-3

Rossi, V. M. & Steel, R. J. (2016). The role of tidal, wave and river currents in the evolution of mixed-energy deltas: Example from the Lajas Formation (Argentina). *Sedimentology*, *63*(4), 824–864. https://doi.org/10.1111/sed.12240

Sassi, M. G., Hoitink, A. J. F., de Brye, B. & Deleersnijder, E. (2012). Downstream hydraulic geometry of a tidally influenced river delta. *Journal of Geophysical Research: Earth Surface*, *117*(F4), n/a-n/a. https://doi.org/10.1029/2012JF002448

Son, S. & Wang, M. (2009). Environmental responses to a land reclamation project in South Korea. *Eos*, *90*(44), 398–399. https://doi.org/10.1029/2009EO440002

Song, D., Wang, X. H., Kiss, A. E. & Bao, X. (2011). The contribution to tidal asymmetry by different combinations of tidal constituents. *J. Geophys. Res*, *116*, 12007. https://doi.org/10.1029/2011JC007270

Speer, P. E. & Aubrey, D. G. (1985). A study of non-linear tidal propagation in shallow inlet/estuarine systems Part II: Theory. *Estuarine, Coastal and Shelf Science*, *21*(2), 207–224. https://doi.org/10.1016/0272-7714(85)90097-6

Stark, J., Smolders, S., Meire, P. & Temmerman, S. (2017). Impact of intertidal area characteristics on estuarine tidal hydrodynamics: A modelling study for the Scheldt Estuary. *Estuarine, Coastal and Shelf Science*, *198*, 138–155. https://doi.org/10.1016/j.ecss.2017.09.004

Toffolon, M. & Lanzoni, S. (2010). Morphological equilibrium of short channels dissecting the tidal flats of coastal lagoons. *Journal of Geophysical Research: Earth Surface*, *115*(4), F04036. https://doi.org/10.1029/2010JF001673

van Rijn, L. C. (2011). Analytical and numerical analysis of tides and salinities in estuaries; part I: tidal wave propagation in convergent estuaries. *Ocean Dynamics*, *61*(11), 1719–1741. https://doi.org/10.1007/s10236-011-0453-0

Van Rijn, L. C. (1993). *Principles of sediment transport in rivers, estuaries and coastal seas* (Vol. 1006). Aqua publications Amsterdam.

Wilson, C., Goodbred, S., Small, C., Gilligan, J., Sams, S., Mallick, B. & Hale, R. (2017). Widespread infilling of tidal channels and navigable waterways in the human-modified tidal deltaplain of southwest Bangladesh. *Elementa*, *5*(0), 78. https://doi.org/10.1525/elementa.263